

# Resonance Structure in the $\gamma\gamma$ Invariant Mass Spectrum in $pC$ - and $dC$ -Interactions

Kh.U. Abraamyan<sup>a,b,\*</sup>, M.I. Baznat<sup>c</sup>, A.V. Friesen<sup>a</sup>, K.K. Gudima<sup>c</sup>, M.A. Kozhin<sup>a</sup>,  
S.A. Lebedev<sup>d,e</sup>, M.A. Nazarenko<sup>a,f</sup>, S.A. Nikitin<sup>a</sup>, G.A. Ososkov<sup>d</sup>,  
S.G. Reznikov<sup>a</sup>, A.N. Sissakian<sup>g</sup>, A.S. Sorin<sup>g</sup>, and V.D. Toneev<sup>g</sup>

a) *VBLHE JINR, 141980 Dubna, Moscow region, Russia*

b) *Yerevan State University, Yerevan, Armeniya*

c) *Institute of Applied Physics, Kishinev, Moldova*

d) *LIT JINR, 141980 Dubna, Moscow region, Russia*

e) *Gesellschaft für Schwerionenforschung, Darmstadt, Germany*

f) *Moscow State Institute of Radioengineering, Electronics and Automation, 119454  
Moscow, Russia*

g) *BLTP JINR, 141980 Dubna, Moscow region, Russia*

## Abstract

Along with  $\pi^0$  and  $\eta$  mesons, a resonance structure in the invariant mass spectrum of two photons at  $M_{\gamma\gamma} = 360 \pm 7 \pm 9$  MeV is observed in the reaction  $dC \rightarrow \gamma + \gamma + X$  at momentum 2.75 GeV/c per nucleon. Estimates of its width and production cross section are  $\Gamma = 63.7 \pm 17.8$  MeV and  $\sigma_{\gamma\gamma} = 98 \pm 24_{-67}^{+93}$   $\mu\text{b}$ , respectively. The collected statistics amount to  $2339 \pm 340$  events of  $1.5 \cdot 10^6$  triggered interactions of a total number  $\sim 10^{12}$  of  $dC$ -interactions. This resonance structure is not observed in  $pC$  collisions at the beam momentum 5.5 GeV/c. Possible mechanisms of this ABC-like effect are discussed.

\*) *abraam@sunhe.jinr.ru*

*Accepted for publication in Phys.Rev.C*

## 1 Introduction

Dynamics of a near-threshold production of the lightest mesons and their interactions, especially the pion-pion interaction, are of lasting interest. A good understanding of the pion-pion scattering is essential as it provides a test for the chiral perturbation theory and the information about quark masses and the chiral condensate. The two-photon decay of light mesons represents an important source of information. In particular, the  $\gamma\gamma$  decay of light scalar mesons was considered as a possible tool to deduce their nature.

Also, the scalar-isoscalar sector is under much debate presently since more states are known (including possible glueball candidates) than can be fitted into a single multiplet. Unfortunately, the existing experimental information from  $\pi\pi$  scattering has many conflicting data sets at intermediate energies and no data at all close to the threshold region of interest. For many years this fact has made it hard to obtain the conclusive results on  $\pi\pi$  scattering at low energies or in the sigma region.

The so-called "ABC effect" is among the oldest and still puzzling problems. Almost fifty years ago Abashian, Booth, and Crowe [1] first observed an anomaly in the production of pion pairs in the reaction  $dp \rightarrow {}^3\text{He} + 2\pi \equiv {}^3\text{He} + X^0$ . This anomaly or ABC effect stands for an unexpected enhancement in the spectrum of the invariant  $\pi\pi$  mass at masses of about 40 MeV higher than  $2m_\pi$ . The subsequent experiments  $dp \rightarrow {}^3\text{He} + X$  [2],  $pn \rightarrow d + 2\pi$  [3, 4, 5],  $dd \rightarrow {}^4\text{He} + X$  [6, 7],  $np \rightarrow d + 2\pi$  with neutron beams [8, 9] and even  $np \rightarrow d + \eta$  [10] independently confirmed this finding. This anomaly was also observed in the photoproduction of pion pairs,  $\gamma p \rightarrow p + X^0$  [11, 12]. It was revealed that the ABC effect is of isoscalar nature since a similar effect was not observed in the  $pd \rightarrow H^3 + X^+$  reaction. The peak positions and widths vary for different bombarding energies and observation angles. Initially, the low-mass enhancement was interpreted as being caused by an unusually strong  $s$ -wave  $\pi\pi$  interaction or as an evidence for the  $\sigma$  meson existence [1] which shortly before was suggested by Johnson and Teller to provide saturation and binding in nuclei [13]. It is usually accepted now that this enhancement is not an intrinsic two-pion property since there is no resonance structure in the  $\pi\pi$  scattering amplitude in this energy range. So any interpretation of the ABC as a real resonance is very much in doubt (for example, see discussion in [8]). It is generally believed that a system like that has to be associated with two nucleons when two pions (both must be present) are rescattered off them or both nucleons participate in elementary  $pp \rightarrow \pi + X$  reactions (predominantly via  $\Delta$  formation). Actually, the origin of the ABC effect must be looked for in the formation of light nuclei at intermediate energies (for a review see Ref. [14]).

The presented complicated situation is reflected in the Particle Data Group (PDG) table [15] where the values quoted for the sigma mass and width, based on both the pole position and the Breit-Wigner parameter determinations, are very widely spread. The estimated mass and half-width are

$$m_\sigma - i\Gamma_\sigma/2 = (400 - 1200) - i(250 - 500) \text{ MeV}. \quad (1)$$

However, during the last years, the chiral perturbation theory and Roy equations led to an accurate description of  $\pi\pi$  scattering at low energies and the precise determination of the mass and width of the  $\sigma$  resonance [16]:

$$m_\sigma = 441_{-8}^{+16} \text{ MeV}; \quad \Gamma_\sigma/2 = 272_{-12.5}^{+9} \text{ MeV}. \quad (2)$$

All experiments conducted on the ABC issue with the exception of low-statistics bubble-chamber measurements [5, 9] were inclusive measurements carried out preferentially with a single-armed magnetic spectrograph for detection of the fused nuclei. They allow one to find the two-pion invariant mass through the missing mass. Very recently, exclusive measurements of reactions  $pd \rightarrow p + d + \pi^0 + \pi^0$  and  $pd \rightarrow {}^3\text{He} + \pi + \pi$  have been carried out with complete kinematics in the energy range of the ABC effect at CELSIUS using the  $4\pi$  WASA detector [17, 18]. The importance of the strongly attractive  $\Delta\Delta$  channel was noted. Surprisingly, the basic  $pp \rightarrow pp\pi^0\pi^0$  reaction in

the  $\Delta\Delta$  region also shows an ABC-like low- $\pi\pi$  mass enhancement which deserves special attention. It confirms the earlier result in [19] where the analyzing powers and cross sections for the ABC enhancement production were measured for the reaction  $\vec{p}p \rightarrow p + p + X^0$  in the missing mass range  $m_\pi^0 < M_{X^0} < m_\eta$ . However, the big difference was observed in the width of the resonance cross section and it was concluded that the observed width in the isoscalar channel is not obviously just a simple result of the binding between the two  $\Delta$  states. It rather signals more complicated configurations in the wave function of the intermediate state, as would be expected for a nontrivial dibaryon state [18].

This work aims to study whether this low- $\pi\pi$  mass anomaly can survive in heavier systems in the  $\gamma\gamma$  channel. The paper is organized as follows. After a brief description of the experiment and experimental setup, the structure of measured invariant mass spectra of photon pairs is analyzed in Sect.2. As a cross-check, a similar analysis is carried out in Sect.3 but within the wavelet method. To elucidate the nature of the peak at  $M_{\gamma\gamma} \approx (2 - 3)m_\pi$ , different mechanisms of the observed  $\gamma\gamma$  pair enhancement are discussed in Sect.4. In Sect.5, experimental estimates for production cross sections and widths of  $\eta$  mesons and hypothetical  $R$  resonance are given. The main inferences of the paper are presented in the Concluding Section.

## 2 Experiment

### 2.1 General layout

The data acquisition of production of neutral mesons and  $\gamma$ -quanta in  $pC$  and  $dC$  interactions has been carried out with internal beams of the JINR Nuclotron [20, 21]. The experiments were conducted with internal proton beams at momentum 5.5 GeV/c incident on a carbon target and with  $^2\text{H}$ ,  $^4\text{He}$  beams and internal C-, Al-, Cu-, W-, Au-targets at moments from 1.7 to 3.8 GeV/c per nucleon. For the first analysis the data with the maximal statistics,  $pC$ - and  $dC$ -interactions, were selected. The first preliminary results on  $dC(2 \text{ AGeV})$  collisions were reported in [21] where some indication on unusual structure in the photon-photon invariant spectrum has been obtained.

The presented data concern reactions induced by deuterons with a momentum 2.75 GeV/c per nucleon and by protons with 5.5 GeV/c. Typical deuteron and proton fluxes were about  $10^9$  and  $2 \cdot 10^8$  per pulse, respectively. The electromagnetic lead glass calorimeter PHOTON-2 was used to measure both the energies and emission angles of photons. The results obtained in earlier experiments with this setup are published in [22]. The experimental instrumentation is schematically represented in Fig.1.

The PHOTON-2 setup includes 32  $\gamma$ -spectrometers of lead glass and scintillation counters  $S_1$  and  $S_2$  of  $2 \times 15 \times 15 \text{ cm}^3$  used in front of the lead glass for the charged particle detection [22, 23, 24].

The center of the front surfaces of the lead glass hodoscopes is located at 300 cm from the target and at angles  $25.6^\circ$  and  $28.5^\circ$  with respect to the beam direction. This gives a solid angle of  $0.094 \text{ sr}$  ( $0.047 \text{ sr}$  for each arm). Some details of the construction and performance of the lead glass hodoscope are given in Tabl.1. The internal target consists of carbon wires with the diameter of 8 micron mounted in a rotatable frame. The overall construction is located in the vacuum shell of the accelerator.

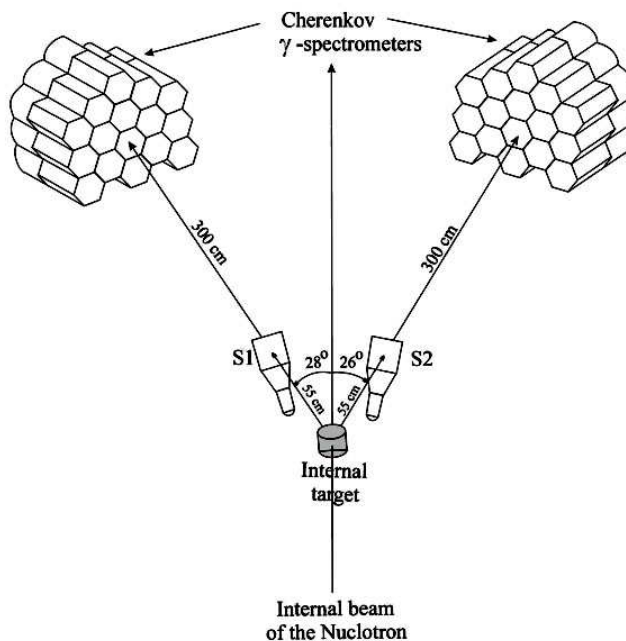


Figure 1: The schematic drawing of the experimental PHOTON-2 setup. The  $S_1$  and  $S_2$  are scintillation counters.

Before the experiment the energy calibration of the lead glass counters has been carried out with 1.5 GeV/c per nucleon deuteron-beam at the JINR synchrotron [23]. The long-term gain stability was continuously monitored for each of the lead glass modules with  $^{32}\text{NaI(Tl)}$  crystals doped with  $^{241}\text{Am}$  sources.

The modules of the  $\gamma$ -spectrometer are assembled into two arms of 16 units. These modules in each arm are divided into two groups of 8 units. The output signals of each group from 8 counters are summed up linearly and sent to the inputs of four discriminators ( $D_i$ ). In this experiment all the discriminator thresholds were at the level of 0.4 GeV. Triggering takes place when there is a coincidence of signals from two or more groups from different arms:  $(D_1 + D_2) \times (D_3 + D_4)$ . In realizing the trigger conditions the amplitudes of all 32 modules were recorded on a disc. The dead time of data acquisition is about 150  $\mu\text{s}$  per trigger. The mean rate of triggering was about 330 and 800 events per spill in  $dC$  and  $pC$  reactions, respectively. Duration of the irradiation cycle is 1 second. Totally about  $1.52 \times 10^6$  and  $1.06 \cdot 10^6$  triggers were recorded during these experiments.

## 2.2 Event selection

Photons in the detector are recognized as isolated and confined clusters (an area of adjacent modules with a signal above the threshold) in the electromagnetic calorimeter. The photon energy is calculated from the energy of the cluster. Cluster characteristics were tested by comparison with Monte-Carlo simulations of electron-photon showers in Cherenkov counters by means of the program package EMCASR [25]. The results obtained earlier with extracted ion beams of the JINR Synchrotron have demonstrated a good agreement between experimental and simulated data [22]. Assuming that the photon originates from the target, its direction is determined from the geomet-

Table 1: The basic parameters of the lead glass hodoscope

Number of lead glasses	32 TF-1, total wight 1422 kg
Module cross section	r=9 cm of insert circumference
Module length	35 cm, 14 R.L.
Spatial resolution	3.2 cm
Angular resolution	0.6°
Energy resolution	(3.9/√E + 0.4)%, E [GeV]
Gain stability	(1-2)%
Dynamic range	50 MeV - 6 GeV
Minimum ionizing signal	382 ±4 MeV of the photon equivalent
Total area	0.848 m <sup>2</sup>

rical positions of constituent modules weighted with the corresponding energy deposit in activated modules.

The invariant mass distributions of photon pairs (from different arms of the spectrometer) are shown in Fig.2. The dominant part of distributions (two upper panels) comes from the  $\pi^0 \rightarrow \gamma\gamma$  decay. These photons in combination with others result in a huge background which mask the expected  $\eta \rightarrow \gamma\gamma$  decay. Other sources of background are charged particles as well as neutrons and particles from a general background in the accelerator hall. Contributions of the given sources were estimated by special measurements with and without veto-detectors *S1* and *S2* and by comparison of data obtained at different beam intensities. The contribution to the total combinatorial spectrum of charged particles, neutrons and particles from a general background in the accelerator hall is less than 10% and becomes negligible (< 1%) after subtraction of mixing event background (see below). As follows from Fig.2, the high-energy cut of photons,  $E_\gamma > 100$  MeV, allows one to improve the signal-to-background ratio. The contribution of the general background in the experimental hall was estimated from the measurements with the empty target, see Fig.3. Two runs carried out for 125 accelerator cycles of the deuteron beam (about  $10^{11}$  deuterons in every run) result in  $N_{\gamma\gamma} = 117428$  and 338 photon pairs for the case with and without target, respectively. So this source contributes less than 1% and is quite smoothly distributed with respect to  $M_{\gamma\gamma}$ .

To see a possible structure of the invariant mass spectra, a background should be subtracted. The so-called event mixing method was used to estimate the combinatorial background: a photon in one event from the first arm is combined with a photon in other events from the second arm. This background was subtracted from the invariant mass distributions (see bottom panels in Fig.2). The background normalization was carried out in two steps. First, the background is normalized to the total pair number (see [21]). Naturally that at the event mixing the resonance maxima are not reproduced disturbing the overall normalization. At the second step this shortcoming of the background estimate is corrected by an auxiliary factor  $K_{norm}$  (which differs by few % from 1) obtained by iterating treatment of the resonance contribution to the spectrum. The negative values in the high-mass range arising at the subtraction of the mixing-event background are caused by the energy conservation law which may be violated when  $\gamma$ -quanta are taken from different mixing events. To decrease its influence the

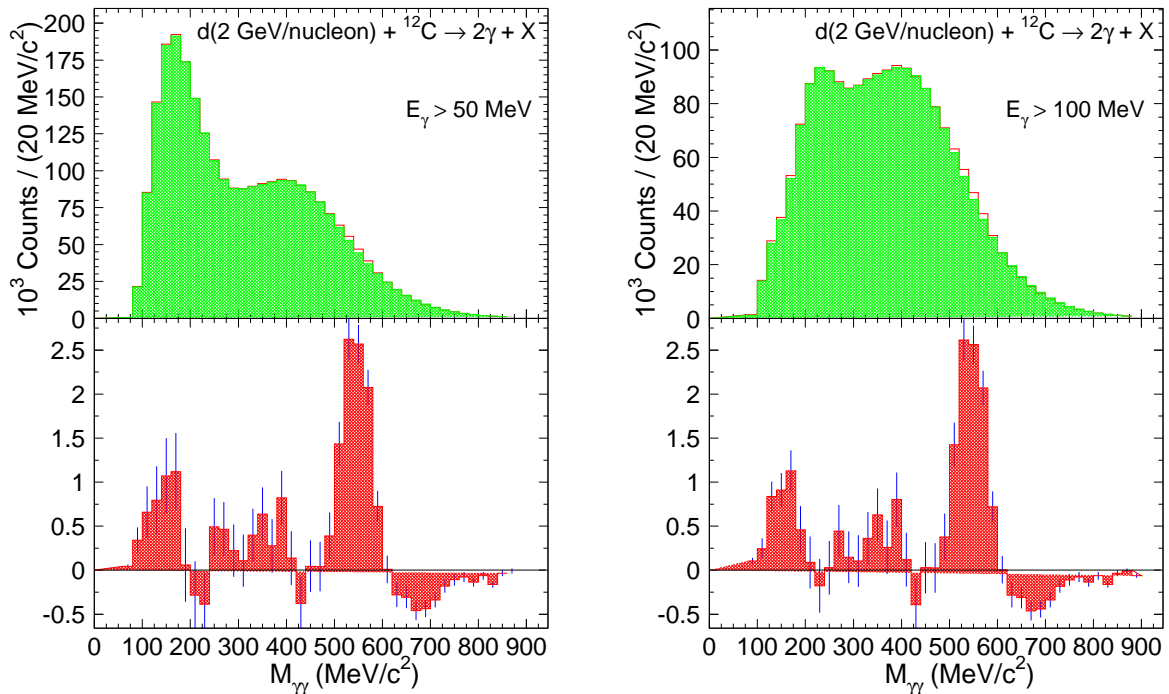


Figure 2: (color online) Invariant mass distribution of  $\gamma\gamma$  pairs from the reaction  $dC \rightarrow \gamma + \gamma + X$  at 2.75 GeV/c per nucleon for two values of the cut energy of photons. The top shaded histograms show the background contribution. The bottom histograms are invariant spectra after the background subtraction. The auxiliary normalization factor  $K_{norm}$  (see below) is 0.9947 for left figure (the cut energy is 50 MeV) and  $K_{norm} = 0.993$  for right figure (the cut energy is 100 MeV).

energy sum of  $\gamma$ -quanta in both individual events and mixing  $\gamma\gamma$  pairs is restricted (see below criterion (3)). A clear peak from the  $\eta$  decay and a remnant of the suppressed  $\pi^0$  resonance are clearly observable. Note that between them there is some additional structure which will be clarified below.

Systematic errors may be due to uncertainty in measurements of  $\gamma$  energies and inaccuracy in estimates of the combinatorial background. The method of energy reconstruction of events is described in detail in Refs. [22, 23]. Possible overlapping effect was studied at higher intensities in CC collisions at the 3.7 GeV per nucleon beam energy. It may result in about 6% displacement of the total mass spectrum. General influence of the overlapping effect in this experiment is very small. One of the criteria of accuracy of energy reconstruction is the conformity of the peak positions corresponding to the known particle mass values. As is seen in Fig.2, the position of peaks corresponding to  $\eta$ - and  $\pi^0$ -mesons is in reasonable agreement with the table values of their masses. A more precise determination of the position of peaks requires minimization of systematic errors in describing the background which arise, in particular, due to the violation of the energy-momentum conservation laws in selecting  $\gamma$ -quanta by random sampling from different events (see also below).

The selection criteria can be made harder by imposing additional trigger conditions. For a background suppression and minimization of systematic errors due to violation of conservation laws the following selection criteria were used:



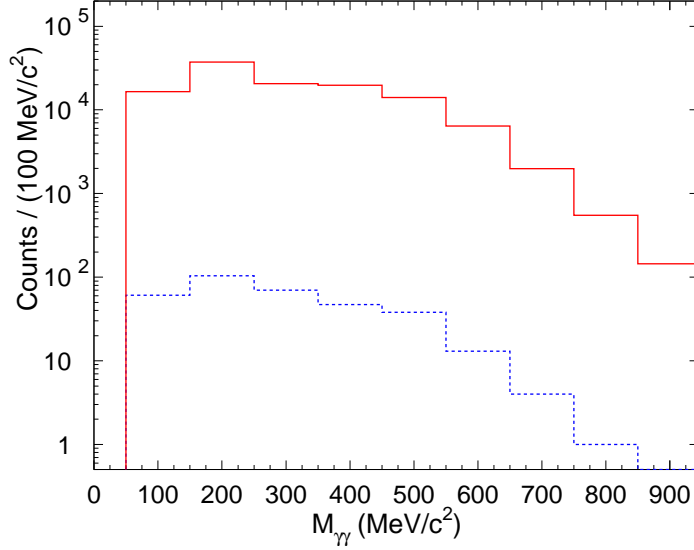


Figure 3: (color online) Invariant mass distributions of  $\gamma\gamma$  pairs in two different runs of measurement under condition  $E_\gamma \geq 50$  MeV: with the empty target (dashed histogram) and with the internal carbon target (solid histogram) in the reaction  $dC = \gamma + \gamma + X$  at 2.75 GeV/c per nucleon.

(1) the number of photons in an event,  $N_\gamma = 2$ ;

(2) the energies of photons,  $E_\gamma \geq 100$  MeV;

(3) the summed energy in real and random events  $\leq 1.5$  GeV. The criterion (1) suppresses the combinatorial background and minimizes systematical errors arisen due to the violation of photon topology at event mixing because events with a different number of photons  $N_\gamma$  have different angular and energy distributions. As noted above, the criterion (2) improves the signal-to-background ratio. The criterion (3) also allows one to minimize systematical errors at event mixing at an insignificant ( $\sim 3\%$ ) loss of events. The result of this triggering is shown in Fig.4. Under the selected condition the  $\pi^0$  peak is practically absent. Therefore,  $\pi^0$ -mesons were mainly detected in events with  $N_\gamma > 2$  (a minimal opening angle of the  $\gamma$  pair detected by the setup equals  $42^\circ$ ). In contrast, the  $\eta$  is seen very distinctly with the width defined by the experimental resolution in the mass. In addition, in this reaction  $dC \rightarrow \gamma + \gamma + X$  a pronounced peak is observed in the interval 300-420 MeV of the invariant mass of two-photon spectrum which will be named below the R-resonance.

However, under similar conditions only  $\eta$  is seen in the  $pC$  collisions. The observed peaks were approximated independently by the Gaussian:

$$\frac{dN}{dM_{\gamma\gamma}} = y_0 + \frac{N_0}{w_{\text{measur}} \sqrt{2\pi}} \exp\left(-\frac{(M_{\gamma\gamma} - M_0)^2}{2w_{\text{measur}}^2}\right). \quad (3)$$

The additional shift-parameter  $y_0$  is introduced in eq.(3). The values of the obtained fitting parameters are given in Tabl.2.

The signal-to-background ratios for the invariant mass intervals of 300-420 MeV and 480-600 MeV (the vicinity of the  $\eta$ -meson mass) are  $2.5 \cdot 10^{-2}$  and  $1.4 \cdot 10^{-1}$ , respectively. For comparison, analogous values without the background suppression (without the selection criteria (1)-(3)) are  $(4.0 \pm 1.4) \cdot 10^{-3}$  and  $3.2 \cdot 10^{-2}$ .

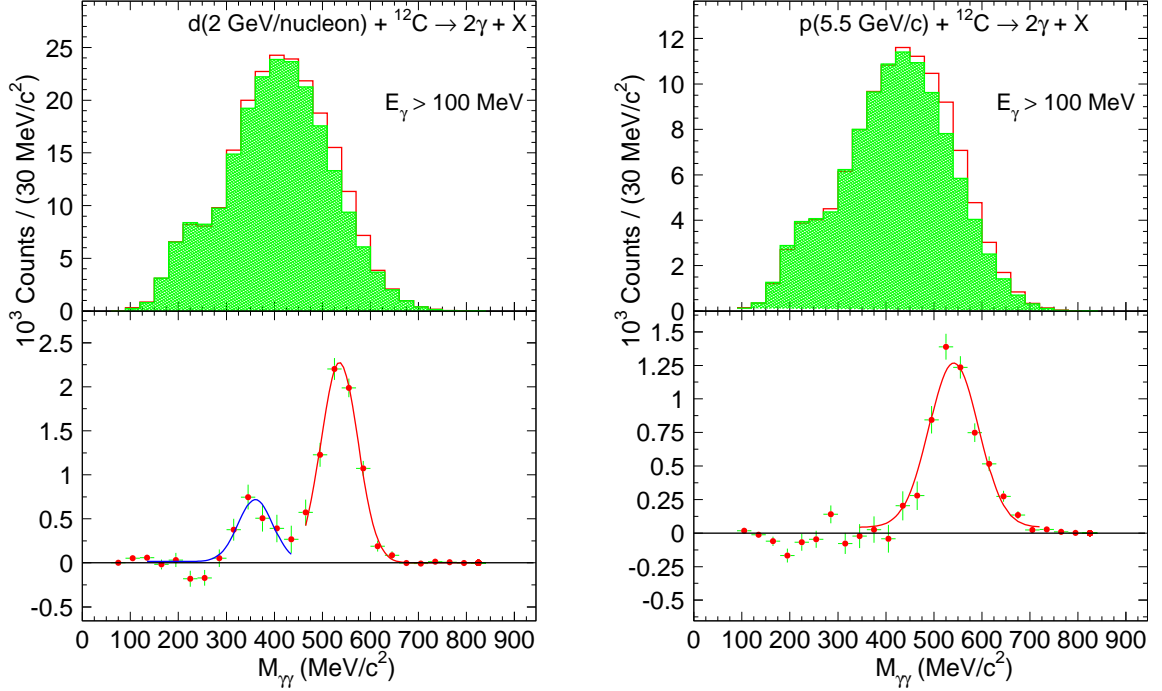


Figure 4: (color online) Invariant mass distributions of  $\gamma\gamma$  pairs satisfying criteria (1) – (3) without (upper panels) and with (bottom panels) the background subtraction obtained for the reaction  $dC \rightarrow \gamma + \gamma + X$  at 2.75 GeV/c per nucleon (left) and  $pC$  collision at 5.5 GeV/c (right), respectively. The curves are the Gaussian approximation of experimental points (see the text). The values of  $K_{norm}$  are 0.958 for  $dC$  and 0.952 for  $pC$ .

Table 2: Fit parameters of the Gaussian distribution

	$dC$ $165 \leq M_{\gamma\gamma} \leq 435$ MeV	$dC$ $465 \leq M_{\gamma\gamma} \leq 825$ MeV
$y_0$	$-1.94 \pm 1.31$	$-0.004 \pm 0.046$
$N_0$	$2623 \pm 472$	$7329 \pm 295$
$w_{measur}$ , MeV	$41.3 \pm 7.2$	$38.5 \pm 1.7$
$M_0$ , MeV/ $c^2$	$362.0 \pm 6.9$	$535.7 \pm 1.9$
$\chi^2$ /degrees of freedom	9.06/6	7.38/9
	$pC$ $345 \leq M_{\gamma\gamma} \leq 645$ MeV	$pC$ $405 \leq M_{\gamma\gamma} \leq 645$ MeV
$y_0$	$1.44 \pm 1.86$	$1.30 \pm 3.07$
$N_0$	$5283 \pm 560$	$4804 \pm 673$
$w_{measur}$ , MeV	$51.6 \pm 4.1$	$41.9 \pm 4.2$
$M_0$ , MeV/ $c^2$	$541.5 \pm 2.5$	$536.6 \pm 2.6$
$\chi^2$ /degrees of freedom	16.10/7	3.13/4



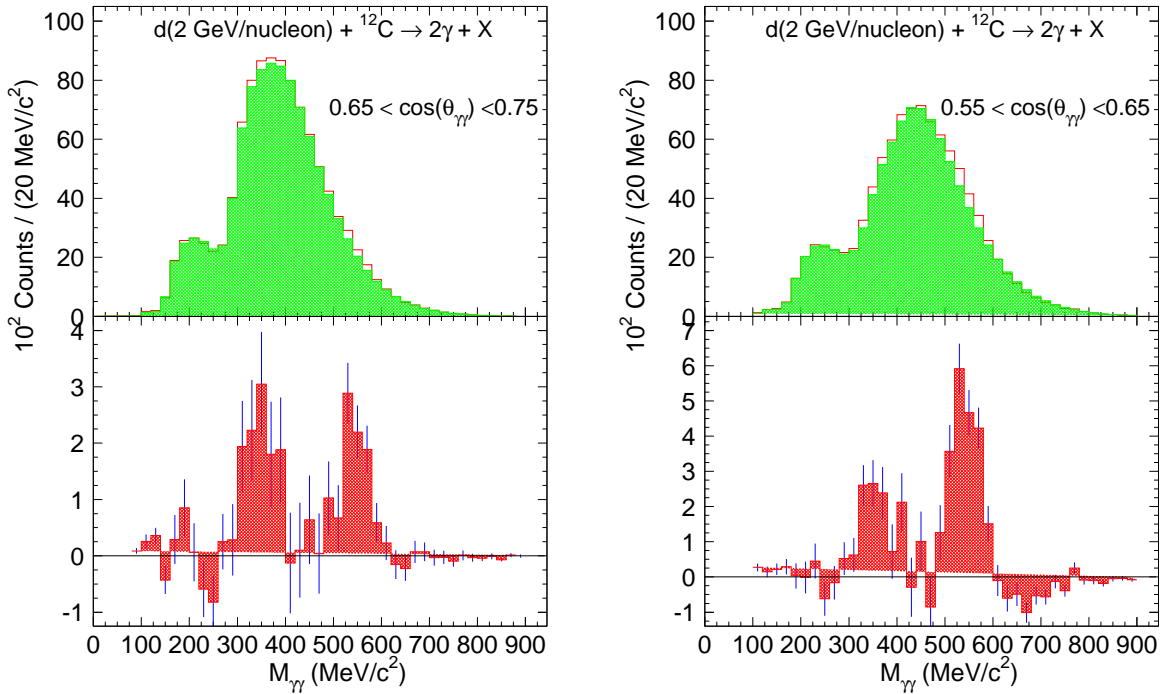


Figure 5: (color online) The invariant mass distributions of two photons for the opening angles  $0.55 < \cos \Theta_{\gamma\gamma} < 0.65$  (left) and  $0.65 < \cos \Theta_{\gamma\gamma} < 0.75$  (right) under the selection criteria (1)  $\div$  (2). The values of  $K_{norm}$  are 0.98 (left) and 0.97 (right).

Thus, as follows from Tabl.2, the position and width of the peak corresponding to  $\eta$ -meson are in good agreement with values from the PDG table (systematic errors do not exceed 2%) and the spectrometer mass resolution. The total number of detected events in the  $dC$  reaction for the  $\eta$ -meson region 450-660 MeV after background subtraction is  $7336 \pm 284$ .

To elucidate the nature of the detected enhancement, we investigate the dependence of its position and width on the opening angle of two photons and on their energy selection level. The results demonstrated in Figs. 5 and 6 show that both maxima survive and are located practically at the same values of  $M_{\gamma\gamma}$ . Pair distributions over the opening angle  $\Theta_{\gamma\gamma}$  for two intervals of the sum of two-photon energy  $0.8 < E_{1\gamma} + E_{2\gamma} < 1.1$  (right) and  $1.1 < E_{1\gamma} + E_{2\gamma} < 1.5$  (left) are displayed in Fig. 7. For lower values of the sum energy the two peaks are seen where the peak at smaller opening angles corresponds to the  $R$  resonance while  $\eta$  mesons are emitted at larger angles around  $\Theta_{\gamma\gamma} \sim 60^\circ$ . Harder energetic selection (left panel) leaves only the  $\eta$  meson contribution.

As is seen, the result of the changing of observation conditions is quite robust: the position and width of the observed peak remain almost unchanged in different intervals of both energies and opening angles of  $\gamma$ -quanta, namely, the mean peak position in the invariant mass distribution varies under different conditions in the range  $348 \div 365$  MeV. The total number of detected events in the region 270-450 MeV (a summed number of pairs in the histogram in Fig.4) after the background subtraction is  $2339 \pm 340$ .

The resonance-like structure observed in invariant mass di-photon distributions is not visible in energy photon spectra. As shown in Fig.8 the  $\gamma$  energy spectra near

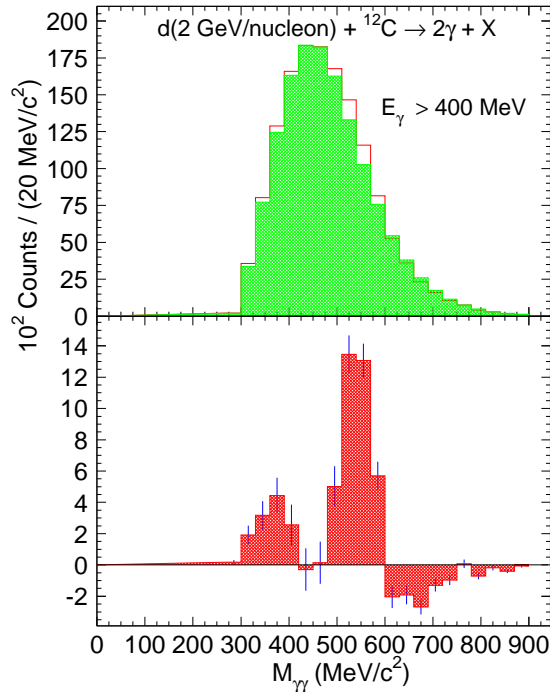


Figure 6: (color online) The invariant mass spectra of  $\gamma\gamma$  pairs for the energy selection  $E_\gamma > 400$  MeV under the selection criteria (1)  $\div$  (2) ,  $K_{norm} = 0.973$ .

the  $R$  resonance are quite smooth, well reproduced by model simulations and have a very similar shape in both arms. This point testifies also that there is no instrumental anomaly causing the  $R$  peak.

Because of smallness of the signal-to-background ratio in the  $R$ -resonance mass range, high statistics is needed for observation. The only most statistically meaningful measurement of the invariant mass spectra was made by the TAPS-collaboration [26]. The closest reaction where the  $\eta$  production was studied is CC interactions at the kinetic energy  $T_C = 2$  AGeV [26]. In this experiment  $13290 \pm 340$  eta mesons were measured but a resonance structure in the range of  $M_{\gamma\gamma} = 300 \div 400$  MeV has not been recorded. If the  $R/\eta$  ratio is assumed to be the same as in the case of  $dC$  collisions, one may expect about  $1800 \cdot (\epsilon_R/\epsilon_\eta)$  of the detected  $R \rightarrow \gamma\gamma$  events, where  $\epsilon_R$  and  $\epsilon_\eta$  are the detection and selection efficiency for  $R$  and  $\eta$ , respectively. Taking into account the systematical uncertainties, this estimated value is in the limits of  $(500 \div 3000) \cdot (\epsilon_R/\epsilon_\eta)$  of the detected  $R \rightarrow \gamma\gamma$  events (see below, formula (10)). The total number of detected events in this range of two-photon invariant masses is about  $6 \cdot 10^5$  [26], so roughly the resonance structure should be observed at the level of  $\sim 1800 \cdot (\epsilon_R/\epsilon_\eta) \pm 800$ . To resolve this structure general statistics should be increased by an order of magnitude, at least. Note that these two experimental setups cover different rapidity regions, which was not taken into account in our estimate. As compared to the TAPS, the PHOTON-2 setup has a smaller angular acceptance but a better signal-to-background ratio. Thus, there is no discrepancy between our result and observation of no resonance structure by the TAPS [26] in the reaction close in the energy and mass numbers.

An indication to a possible resonance structure in pp-collisions at the energies 1.36 and 1.2 GeV was obtained by the CELSIUS-WASA collaboration [52]. However

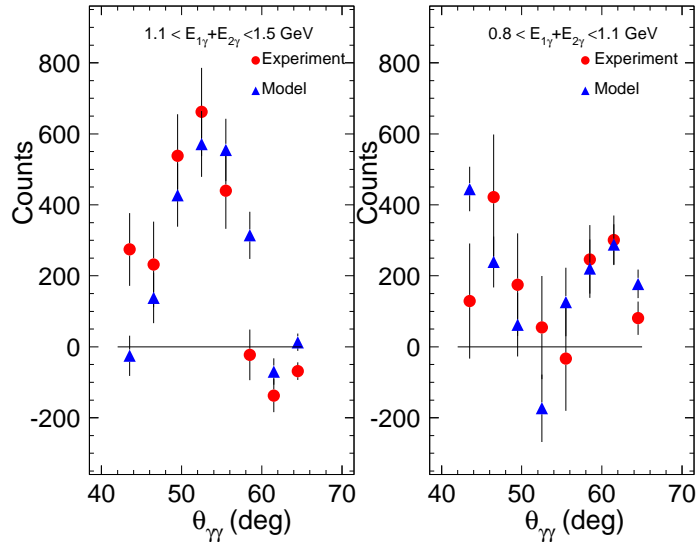


Figure 7: (color online) Distribution of the opening angle of  $\gamma\gamma$  pairs in  $dC$  collisions for the two selections of  $(E_{1\gamma} + E_{2\gamma})$ . Other conditions are the same as in Fig.4. Experimental (circles) and simulated (triangles) results are normalized to the same number of photon pairs. The values of  $K_{norm}$  are 0.974 (left) and 0.99 (right).

statistics in the invariant mass range 250-350 MeV is low: only about 200  $\gamma\gamma$  pairs without background subtraction was found.

### 3 Wavelet analysis

Here we shall try to identify essential structures in the measured  $M_{\gamma\gamma}$  spectra without the background subtraction. A conventional method for such analysis is a wavelet transformation which is known as an efficient multiscale technique to reduce the presence of statistical noise and then extract physical parameters from the obtained smoothed form [27, 28]. The one-dimensional wavelet transform (WT) of a signal  $f(x)$  has a biparametric form. This allows WT to overcome the main shortcomings of the Fourier transform such as nonlocality, infinite support and necessity of a broad band of frequencies to decompose even a short signal. The wavelet transformation changes the decomposition basis into functions which are compact into a time/space and frequency domain. The WT with the wavelet function  $\psi$  of the function  $f(x)$  is defined by convolution as

$$W_{\psi}(a, b)f = \frac{1}{\sqrt{C_{\psi}}} \int_{-\infty}^{\infty} \frac{1}{\sqrt{|a|}} \psi\left(\frac{b-x}{a}\right) f(x) dx \quad (4)$$

with the normalization constant

$$C_{\psi} = 2\pi \int_{-\infty}^{\infty} \frac{|\tilde{\psi}(\omega)|^2}{|\omega|} d\omega < \infty,$$

where  $\tilde{\psi}(\omega)$  is the Fourier transform of the wavelet  $\psi(x)$ . A scale parameter  $a$  characterizes the dilatation and  $b$  is the translation in time or space. In this respect the

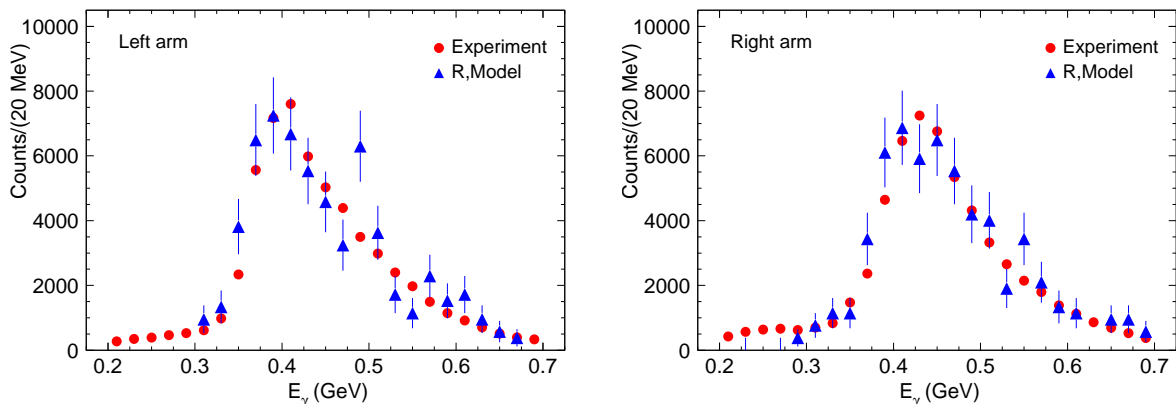


Figure 8: (color online) Photon energy spectra from  $\gamma\gamma$  pairs in the invariant mass interval  $\Delta M_{\gamma\gamma} = 0.32 \div 0.4$  GeV. Experimental (circles) and Monte-Carlo simulation (triangles) points calculated with inclusion of the  $R$  resonance formation are given separately for every spectrometer arm. Distributions are normalized to the same total number of events.

wavelet function  $\psi(t)$  is a sort of a "window function" with a non-constant window width: high-frequency events are narrow (due to the factor  $1/a$ ), while low-frequency wavelets are broader. The inverse transform is given by the formula

$$f(t) = C_\psi^{-1} \int \int \psi\left(\frac{t-b}{a}\right) W_\psi(a, b) \frac{da db}{a^2}. \quad (5)$$

The wavelet  $\psi$  exists if  $C_\psi < \infty$ . It holds, in particular, when the first  $(n-1)$  moments are equal to zero

$$\int_{-\infty}^{\infty} |x|^m \psi(x) dx = 0, \quad 0 \leq m < n. \quad (6)$$

Due to freedom in the choice of the wavelet function  $\psi$ , many different wavelets were invented [29, 30]. We consider here only continuous Wavelets with Vanishing Moments (WVM) (see it Appendix A). The WVM family is called so because condition (6) always holds for it. One of WVM families is a set of *Gaussian wavelets* (GW) which are normalized derivatives of the Gauss function

$$g(x; A, x_0) = A \exp\left(-\frac{(x-x_0)^2}{2\sigma^2}\right). \quad (7)$$

In some cases continuous wavelets are more suitable to evaluate peak parameters. One of these cases arises when a peak in question has a Gaussian shape (7). This makes it possible to use very simple analytical expressions, eq.(19), in the continuous Gaussian wavelet transform for Gaussian peaks. It gives us a remarkable advantage to calculate the peak parameters directly in the wavelet domain instead of the time/space domain *without using the inversion*. Moreover, in real cases, when our signal shape is close to a Gaussian one and is considerably contaminated by an additive noise and, in addition, is distorted by binning to be input to computer, one can also use the remarkable robustness of Gaussian wavelet filtering, as proved in [30].

Wavelet ability to separate signal components with different frequencies and positions has attracted many physicists to use both discrete and continuous wavelets [33, 34]. Usually the conventional filtering approach is applied: a signal transformed by a wavelet undergoes an appropriate thresholding and then is restored by the inverse transform. The image of the wavelet spectrum is used to obtain rough parameter estimations of wanted peaks of invariant mass spectra, as in [35] where the Mexican hat wavelet was used. In our paper, we apply the family of GW to look for peaks in question having a Gaussian shape (7).

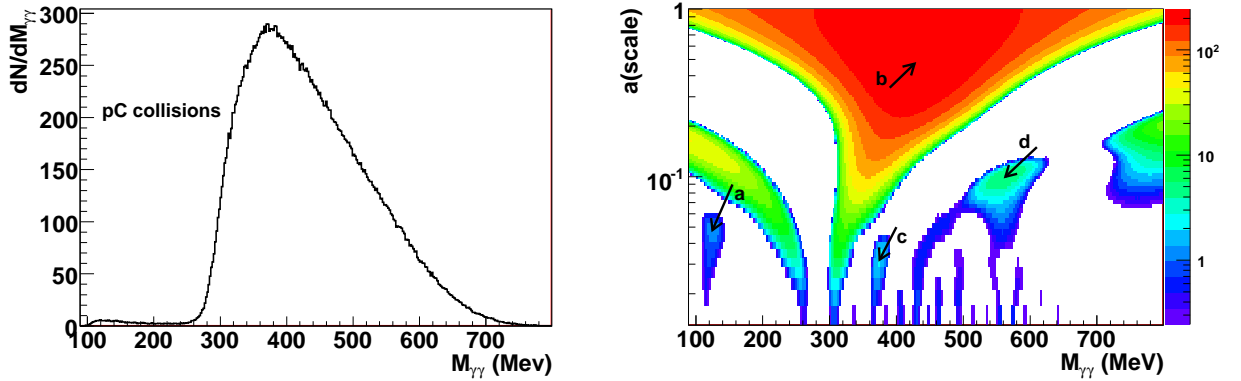


Figure 9: (color online) The invariant mass distribution of  $\gamma\gamma$  pairs (top) and the biparametric distribution of the GW of the 8-th order (bottom) for  $pC$  interactions. These events are selected under the same conditions as in Fig.4 but the distribution is obtained with an additional condition for photon energies  $E_{\gamma_1}/E_{\gamma_2} > 0.8$  and binning in 2 MeV.

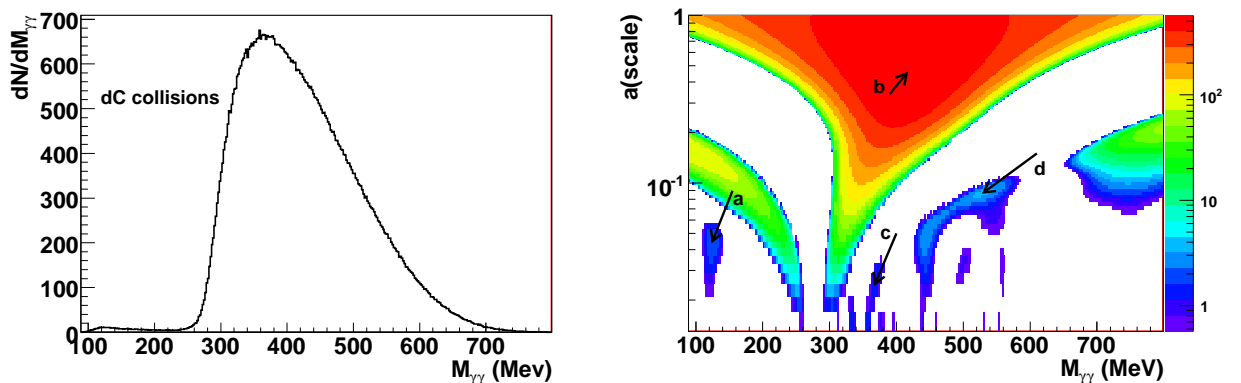


Figure 10: (color online) The same as in Fig.9 but for  $dC$  collisions.

The main idea of our approach is to transform the signal  $f(x)$  to the space of the corresponding wavelet and look there for a local biparametric area surrounding the wavelet image of our peak in question, drawing down all other details of the signal image, concerning noise, binning effects, and background pedestal. A particular example of the  $G_2(a, b)$  transform and other details of this analysis are given in *Appendix A*.

The initial signal  $f(x)$ , *i.e.* the  $M_{\gamma\gamma}$  distribution including the background is presented in the upper panels of Figs.9 and 10. Here an additional condition on photon

energies  $E_{\gamma 1}/E_{\gamma 2} > 0.8$  (where  $E_{\gamma 1}$  and  $E_{\gamma 2}$  are the smallest and the largest energy in the given photon pair, respectively) was applied to data to improve the signal-to-background ratio and avoid double-humped structure which will require higher orders of the expansion. The distributions look quite smooth due to the choice of a smaller step in  $M_{\gamma\gamma}$  which is needed to provide more points for the wavelet analysis.

The wavelet transformation results are presented in the lower panels of Figs. 9 and 10 for  $pC$  and  $dC$ , respectively. Assuming symmetric signal we use the WVM of the 8-th order to separate noise and see a peak structure. Attempts to apply wavelets of lower than 8-th order give worse results, perhaps, because of rather ragged signals. The arrows show an approximate location of the identified peaks. Due to the trigger condition, the distribution maximum ( $a$ ) of photons from the  $\pi^0$  decay is shifted to  $M_{\gamma\gamma} \sim 125$  MeV from the expected 135 MeV. It is in agreement with the initial distribution shown in the same figures. A huge peak from the background ( $b$ ) dominates and its shape is quite close to the Gaussian. A photon peak from the  $\eta$  decay, ( $d$ ), is seen quite distinctly at the proper place but its intensity is suppressed due to an additional condition  $E_{\gamma 1}/E_{\gamma 2} > 0.8$ . In the domain of interest there is some enhancement near  $M_{\gamma\gamma} \sim 370$  MeV marked in the figures by ( $c$ ). In the biparametric representation this spot has not a circle shape because even in the case of a coarse binning it is not well approximated by the Gaussian (see Tabl.2). In this respect, the ( $c$ )-peak in  $pC$  seems to be more pronounced than the appropriate one in  $dC$  but it follows from lower statistics in the  $pC$  case where a separate point may be better approximated by the Gaussian. Note that statistics in these cases differs by the factor of more than 3. The WVM analysis still reveals one more weak ( $c$ )-peak at higher  $M_{\gamma\gamma}$ . This is not very surprising since in coarse binning (see Fig.2) they were blurred but they are seen at a more strict selection (cf. Figs.4 ÷ 6).

Therefore, the presented results of the continuous wavelet analysis with vanishing moments confirm the finding of a peak at  $M_{\gamma\gamma} \sim (2-3)m_\pi$  in the  $\gamma\gamma$  invariant mass distribution obtained within the standard method with the subtraction of the background from mixing events.

## 4 Data simulation

### 4.1 About the model

To simulate  $pC$  and  $dC$  reactions we use a transport code. At high energies it is the Quark-Gluon String Model (QGSM) [36] and at the energy of a few GeV the string dynamics is reduced to the earlier developed Dubna Cascade Model (DCM) [37] with upgrade of elementary cross sections involved [38].

The DCM divides the collision into three stages, well separated in time. During the first initial stage an intranuclear cascade develops, primary particles can scatter and secondary particles can re-scatter several times prior to their absorption or escape from the nucleus. At the end of this step the coalescence model is used to localize  $d$ ,  $t$ ,  $^3\text{He}$ , and  $^4\text{He}$  particles from nucleons found inside spheres with well-defined radii in configuration space and momentum space. The emission of cascade particles determines a particle-hole configuration, i.e.,  $Z, A$ , and excitation energy that is taken as the starting point for the second, pre-equilibrium stage of the reaction, described according to the cascade exciton model [39]. Some pre-equilibrium particles may be



emitted and this leads to a lower excitation of the thermalized residual nuclei. In the third, final evaporation/fission stage of the reaction, the de-excitation of the residue is described with the evaporation model. The last two stages are important for triggering the events. All components contribute normally to the final spectra of particles and light fragments; low-energy evaporated photons are not included into subsequent analysis. For relativistic energies the cascade part of the DCM is replaced by the refined cascade model, which is a version of the quark-gluon string model (QGSM) developed in [40] and extended to intermediate energies in [41]. The description of the mean-field evolution is simplified in the DCM in the sense that the shape of the scalar nuclear potential, defined by the local Thomas-Fermi approximation, remains the same throughout the collision. Only the potential depth changes in time, according to the number of knocked-out nucleons. This frozen mean-field approximation allows us to take into account the nuclear binding energies and the Pauli exclusion principle, as well as to estimate the excitation energy of the residual nucleus by counting the excited particle-hole states. This approximation is usually considered to work particularly well for hadron-nucleus collisions.

The following  $\gamma$ -decay channels are taken into account: the direct decays of  $\pi^0, \eta, \eta'$  hadrons into two  $\gamma$ 's,  $\omega \rightarrow \pi^0\gamma$ ,  $\Delta \rightarrow N\gamma$  and the Dalitz decay of  $\eta \rightarrow \pi^+\pi^-\gamma$ ,  $\eta \rightarrow \gamma e^+ + e^-$  and  $\pi^0 \rightarrow \gamma e^+ + e^-$ , the  $\eta' \rightarrow \rho^0 + \gamma$ , the  $\Sigma \rightarrow \Lambda + \gamma$ , the  $\pi N$  and  $NN$ -bremsstrahlung. One should note that in accordance with the recent HADES data [42], the  $pn$ -bremsstrahlung turned out to be higher by a factor of about 5 than a standard estimate and weakly depends on the energy. This finding, being in agreement with the recent result of Ref.[43], allowed one to resolve the old DLS puzzle [44]. This enhancement factor is included in our calculations.

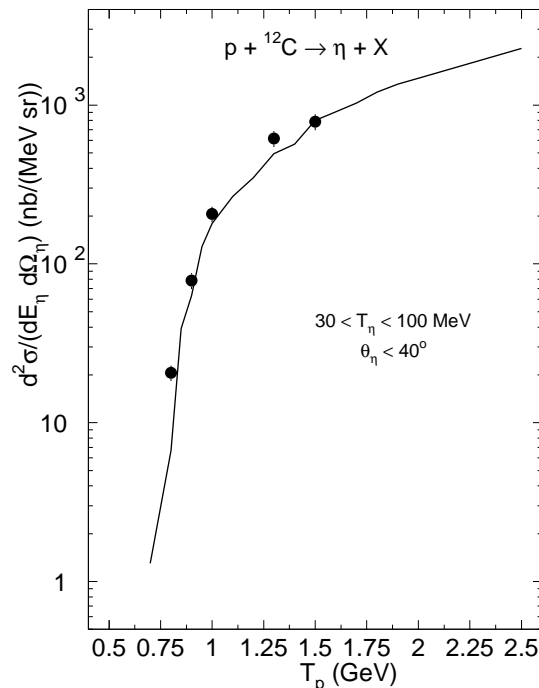


Figure 11: The proton energy dependence of the double differential cross section for the  $\eta$  production in  $pC$  collisions. Experimental points are from [45].

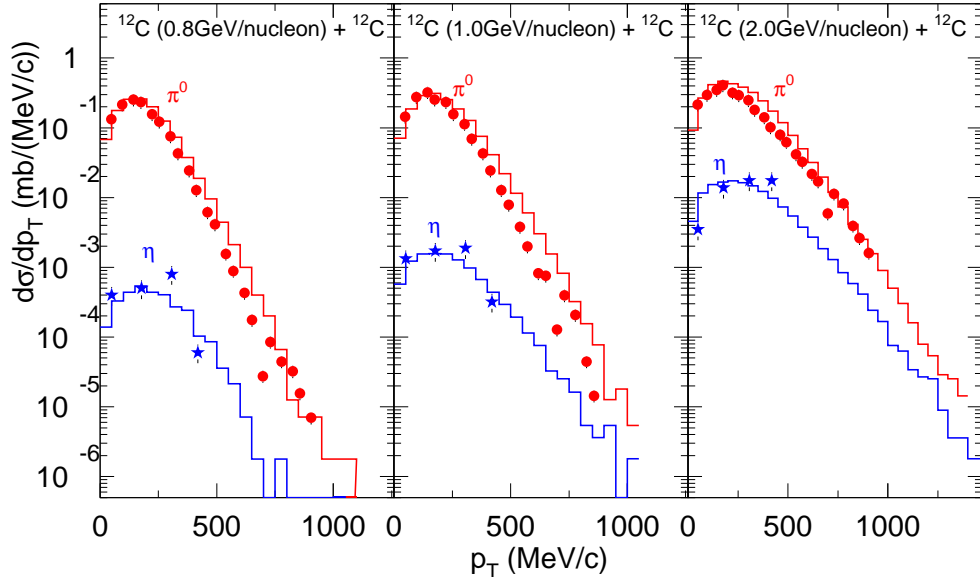


Figure 12: (color online) Transverse momentum distributions of  $\pi^0$  and  $\eta$  in the middle rapidity range from  $CC$  collisions at different energies. Experimental points are from the TAPS Collaboration [26].

As a model test, in Fig.11 the excitation function for the  $\eta$  production is shown for the  $pC$  collisions. The model describes correctly a fast increase of the  $\eta$  yield near the threshold where the cross section is changed by two orders of magnitude.

The transverse momentum distributions at the mid-rapidity are presented in Fig.12 for  $\pi^0$  and  $\eta$  produced in  $CC$  collisions at three bombarding energies. The model results are in good agreement with the TAPS experiment [26] for both neutral pions and eta mesons. So this gives us some justification for application of our model to analyze neutral particle production in the reactions considered.

## 4.2 Analysis of the obtained data

The model described above is implemented for describing the measured distributions with careful simulations of experimental acceptance. The total statistics of simulated events amounts to about  $10^9$  here and in every case below. As is seen from Fig.13, the model reproduces quite accurately the observed  $\eta$  peak in the invariant mass distribution of  $\gamma$  pairs but there is no enhancement in the region of the  $R$ -resonance.

The mass of the  $R$  resonance is slightly above  $2m_\pi$ . As was noted, there is no particularities in the phase shifts for the  $\pi\pi$  scattering. We remind that according to the PDG table [15], the closest-in-mass hadron in this energy range is the  $f_0(600)$ -meson (or the  $\sigma$ -meson) with the extended mass and very large width (see eq.(1)); however, the recent analysis gives a more defined  $\sigma$  mass and a more narrow width (see eq.(2)).

To see whether such a resonance structure would be created due to a nuclear interaction and can survive in the strict experimental conditions, we artificially simulate

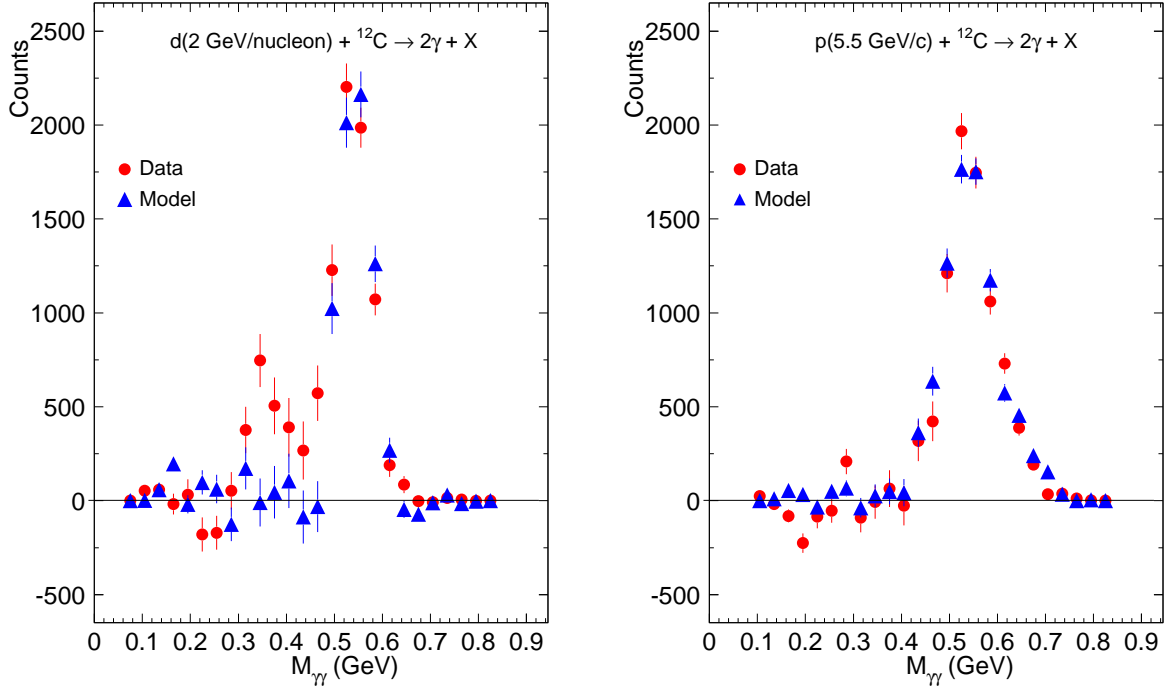


Figure 13: (color online) The invariant mass distributions of  $\gamma\gamma$  pairs from the  $dC$  (left) and  $pC$  (right) reactions after background subtraction. Both experimental (circles) and simulated (triangles) points are obtained under the same PHOTON-2 conditions.

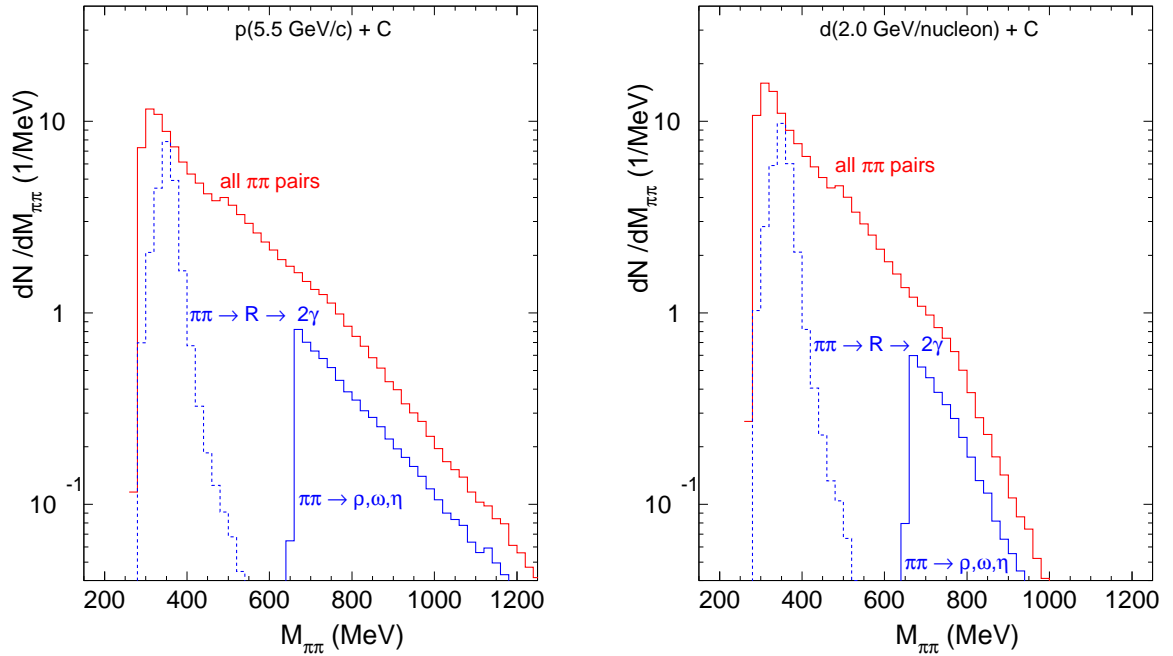


Figure 14: Invariant mass distribution of pion pairs from  $\pi\pi$  interactions in  $pC$  (left) and  $dC$  (right) collisions. The contributions resulting in the  $R$ -resonance and formation of  $\rho, \omega, \eta'$  mesons are shown separately.

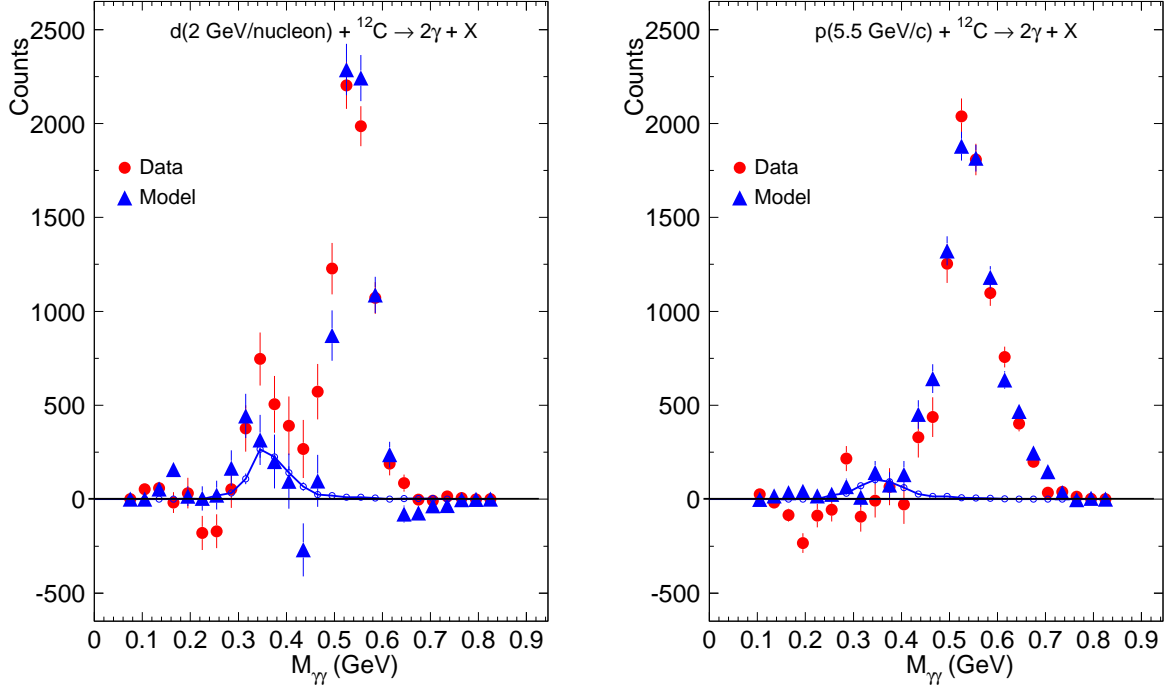


Figure 15: (color online) Invariant mass distributions of  $\gamma\gamma$  pairs from the  $dC$  and  $pC$  reactions after background subtraction. Both experimental (circles) and simulated (triangles) points are obtained under the same conditions. The contribution of photons from the  $R$  decay is shown by the solid line.

production of the  $R$ -resonance and follow its fate in the course of a nuclear collision. It is assumed that the putative  $R$  resonance can be created in every  $\pi^+\pi^-$  or  $\pi^0\pi^0$  interaction if its invariant mass  $M_{\pi\pi}$  satisfies the Gaussian distribution with the observed parameters (see Tabl.2). The  $M_{\pi\pi}$  distributions for proton- and deuteron-induced reactions is presented in Fig.14. These distributions are rather wide with a pronounced peak in the region of  $(2-3)m_\pi$ . The fraction of interactions identified with the formation of the  $R$ -resonance is slightly above 20 % of all  $\pi\pi$  collisions. Interactions with  $M_{\pi\pi} \sim 650$  MeV resulting in heavy mesons  $\rho, \omega, \eta$  come to about 5 %.

If the  $R$  resonance has been formed, it is assumed to decay only in two photons. This scheme can be easily realized by the Monte Carlo method within our transport model. The two-photon invariant mass spectra calculated with the inclusion of the possible  $R$  production are compared with experiment in Fig.15. Indeed, the essential part of  $\gamma\gamma$  pairs survives through the strict selected rules and can explain (20 – 30)% of the enhancement in the case of  $dC$  collisions. For  $pC$  collisions the  $R$  contribution is smaller but in agreement with experimental points. Nevertheless, one should be careful in taking too seriously the absolute values of the  $\gamma\gamma$  pair yields estimated from the  $R$  decay. They are obtained under extreme assumption that all  $R$  resonances do decay via the two-photon channel, *i.e.*  $\Gamma_R = \Gamma_{\gamma\gamma}$ . However, the scalar resonance (like the  $\sigma$  meson) decays mainly into two pions,  $\Gamma_R = \Gamma_{\pi\pi}$ , and the electromagnetic decay is strongly suppressed. The two-photon decay is dominating ( $\Gamma_R = \Gamma_{\gamma\gamma}$ ) only if the  $R$  mass is below the two-pion threshold. So the proposed mechanism allows one to consider properly the kinematics of the  $\gamma\gamma$  pairs and the role of acceptance, but it is

not able to describe the absolute  $R$  yield which should be by a few orders of magnitude lower than that presented in Fig.15.

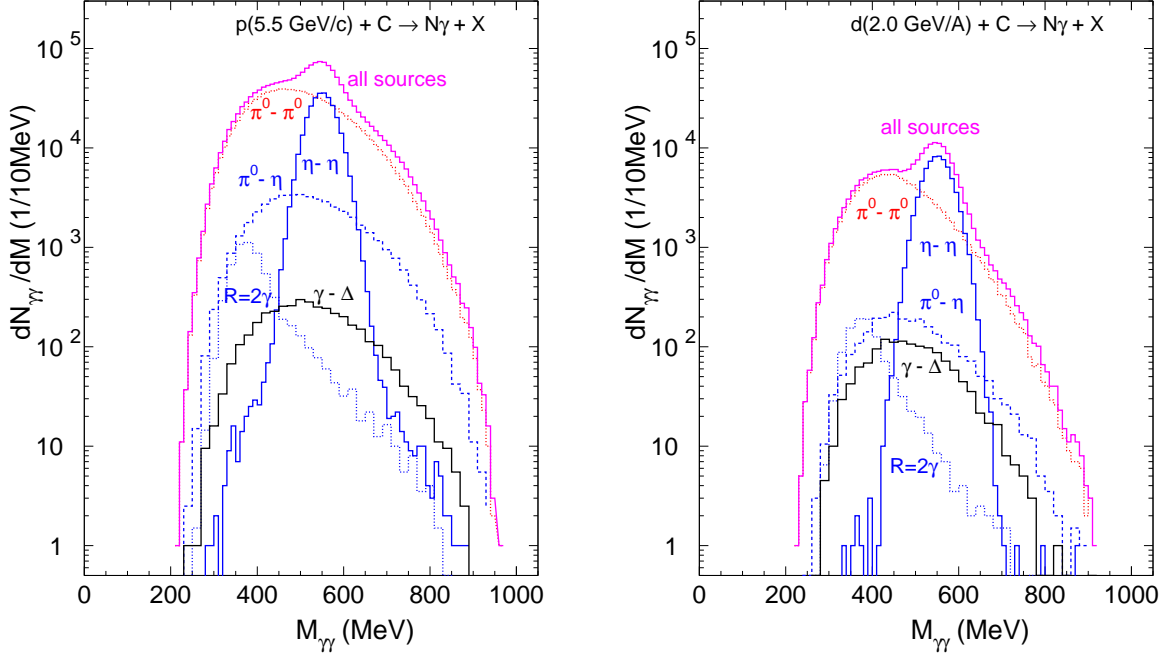


Figure 16: (color online) The calculated  $\gamma\gamma$  invariant mass distribution in  $pC$  (left) and  $dC$  (right) collisions for selected events with  $N_\gamma = 2$ . Contributions of different channels are shown. Symbols near curves describe sources which photons originate from.

Model simulation allows us to disentangle different  $\gamma$  sources to clarify the production mechanisms. This is illustrated in Fig.16. The double symbol near curves indicates the sources where both photons came from. The  $\pi^0$  decay (marked as " $\pi^0 - \pi^0$ " in figures) naturally dominates in both the reactions. In the energy range considered, the pion yield rapidly increases and due to that a number of  $\gamma\gamma$  pairs is higher in the  $pC$ (4.6 GeV) than in the  $dC$ (2 AGeV) collisions. The  $\eta$  decay (" $\eta - \eta$ ") is seen clearly, being spread essentially due to uncertainties in the  $\gamma$  energy measurement. In the  $dC$  case the  $\eta$  maximum is more pronounced in the total distribution. It is of interest that the  $R$  resonance decay (" $R \rightarrow 2\gamma$ ") is also visible under PHOTON-2 conditions. A number of  $\gamma\gamma$  pairs from  $R$  is higher in the  $pC$  case, but the ratios for  $\eta/R$  are comparable:  $\eta/R= 34.18$  and  $24.95$  for  $dC$  and  $pC$  collisions, respectively. It means that a possibility to observe the  $R$  resonance depends on statistics of measured events.

One should note that since the low-mass enhancement in the invariant  $\pi\pi$  spectra showed up clearly at beam energies corresponding to the excitation of  $\Delta$ 's in the nuclear system, the ABC effect was interpreted by a  $\Delta\Delta$  excitation [46, 47]. In particular, the early simplest model for ABC production in  $pn \rightarrow d + X^0$  involves the excitation of both nucleons into  $\Delta$ -isobars through a one-pion exchange where, after the decay of two  $\Delta$ 's, the final neutron-proton pair sticks together to produce the observed deuteron [46]. Though the enhancement observed in the inclusive data for the  $\pi^0\pi^0$  channel turns out in some cases to be much larger than the predicted in these calculations,

the  $\Delta\Delta$  mechanism is still attractive. More delicate results on the vector and tensor analyzing powers in  $\bar{d}d \rightarrow {}^4\text{He} + X^0$  give strong quantitative support to this idea [7]

The channel marked in Fig.16 as " $\gamma-\Delta$ " corresponds to the case when photons from the  $\Delta$  decay correlate with any other. Though the two-photon yield for this channel in the  $dC$  case is close to that from the  $R$  decay, the maximum location is shifted to higher  $M_{\gamma\gamma}$  by more than 100 MeV. If one chooses both the photons from different  $\Delta$  isobars, for the PHOTON-2 conditions we have none event from  $10^9$  of simulated ones. One should note that we consider incoherent  $\Delta\Delta$  interactions and possible attraction in this channel is not taken into account.

### 4.3 The $\eta \rightarrow 3\pi^0$ decay

As was indicated many years ago, a three-pion resonance having the mass  $M_\eta = 550$  MeV and isospin  $T = 0$  maybe a pseudoscalar particle of positive  $G$  parity ( $0^{-+}$ ). Under this assumption it was shown that the partial rates and widths for this  $\eta$  decay will be consistent with available experimental data providing that the  $\eta \rightarrow 3\pi$  channel is enhanced by a strong final state interaction [48]. This strong interaction is realized by postulating the existence of a particle having the spin and parity  $0^+$  and called a  $\sigma$ . Then the  $3\pi$  decay of the  $\eta$  meson would proceed in two distinct steps:  $\eta \rightarrow \sigma + \pi^0$ ,  $\sigma \rightarrow 2\pi^0$  or  $(\pi^+\pi^-)$  where the first step is an electromagnetic decay, while the second occurs through the strong interaction. The fit to experimental data gives the mass of a  $\sigma$  particle about 370 MeV and a full width of about 50 MeV [48]. These parameters coincide with those extracted from the direct analysis of pion spectra from the  $3\pi$  decay of the  $\eta$  meson [49, 50]. The enhancement of the  $3\pi$  channel was argued by the presence of a strong two-pion interaction which resembles the ABC effect. It is of interest that the presence of such a pion-pion resonance improves also the calculation of the  $K_L - K_S$  mass difference [51].

To check this mechanism (see Fig.17) we simulated two channels of the  $\eta$  decay: the direct decay into two photons  $\eta \rightarrow 2\gamma$  and  $\eta \rightarrow 3\pi^0$  which then decay into photons. The last channel was calculated under two assumptions. The first, all the three pions decay independently,  $\pi^0 \rightarrow \gamma\gamma$ , creating 6 photons. The second version assumes that, as discussed above, two pions may interact forming  $\sigma$  which decay into 2 pions, so  $\eta \rightarrow \sigma + \pi^0 \rightarrow 6\gamma$ . As it is seen (bottom panels in Fig.17), the interaction in the  $\pi\pi$  channel results in some enhancement in the  $\pi\pi$  invariant mass spectra as compared the noninteracting case. The  $\gamma\gamma$  invariant mass spectra exhibit a spread maximum near the pion mass and they are practically identical in both the cases (dashed lines). If the PHOTON-2 selection conditions are implemented, a clear signal (solid lines in Fig.17) at  $M_{\gamma\gamma} \sim 350$  MeV appears but its intensity is by about three orders of magnitude lower than that for the  $\eta$  meson. It is of interest that the absolute values and shape of the  $M_{\gamma\gamma}$  spectrum are again very similar in both the versions. So in the  $\eta \rightarrow 3\pi^0$  decay it is hardly ever possible to disentangle the cases with and without the two-pion interaction by the detection of decay photons.

### 4.4 Dibaryon mechanism

Recently, a resonance-like structure has been found by the CELSIUS-WASA Collaboration in the two-photon invariant mass spectrum near  $M_{\gamma\gamma} \sim 2m_\pi$  of the exclusive reaction  $pp \rightarrow pp\gamma\gamma$  at 1.2 and 1.36 GeV [52]. This observation was interpreted as  $\sigma$



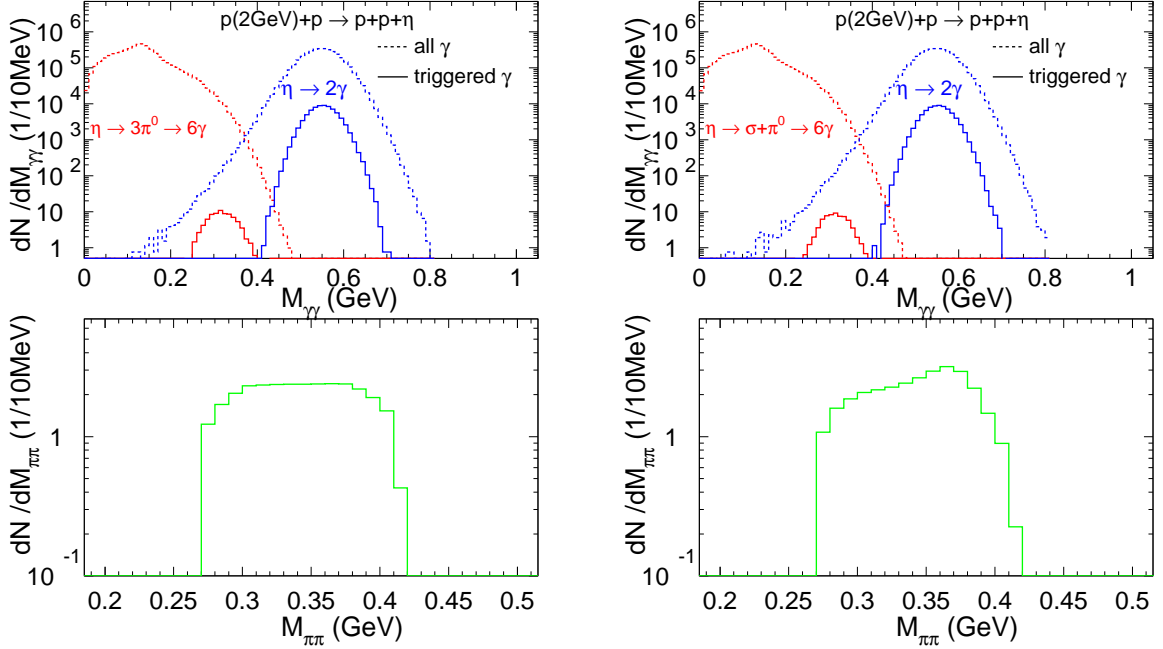


Figure 17: (color online) The  $\gamma\gamma$  (top) and  $\pi\pi$  (bottom) invariant mass distributions for the  $\eta$  decay through the  $\eta \rightarrow \gamma\gamma$  and  $\eta \rightarrow 3\pi^0$  channels from pp collisions. The left panels correspond to the  $\eta \rightarrow 3\pi^0 \rightarrow 6\gamma$  mechanism, results in the right panels include interaction of two pions via the  $\sigma$  meson,  $\eta \rightarrow \sigma + \pi^0 \rightarrow 6\gamma$ . The dashed lines are calculated for the full  $4\pi$  acceptance, the solid lines take into account the PHOTON-2 kinematical conditions.

channel pion loops which are generated by the  $pp$  collision process and decay into the  $\gamma\gamma$  channel. Interference with the underlying double bremsstrahlung background can give a reasonable account of data[52].

In Ref.[53], some arguments were given that such an interpretation is at least questionable and an alternative explanation was proposed where a possible origin of the structure is based on the dibaryon mechanism of the two-photon emission [54]. The proposed mechanism  $NN \rightarrow d_1^* \rightarrow NN\gamma\gamma$  proceeds through a sequential emission of two photons, one of which is caused by production of the decoupled baryon resonance  $d_1^*$  and the other is its subsequent decay. The  $pp \rightarrow pp\gamma\gamma$  transition is treated in [53] within the assumption that at a large distance the  $NN$ -decoupled six quark  $d_1^*$  state is a bound  $p\Delta(1232)$  state with the spin-parity  $J^P = 0^-$  and isospin  $I = 2$  [55]. The matrix elements were estimated phenomenologically and effects of the final state interactions between decay protons were included. This model reproduces reasonably well the experimentally observed  $M_{\gamma\gamma}$  spectrum of the  $pp \rightarrow pp\gamma\gamma$  reaction in the vicinity of the resonance structure [53].

We would like to check whether this dibaryon mechanism may be responsible for the peak observed in the  $M_{\gamma\gamma}$  distribution of the  $dC$  collisions at  $T = 2$  AGeV. The two-step scheme  $NN \rightarrow d_1^*\gamma \rightarrow NN\gamma\gamma$ , where the dibaryon mass is  $m_d = m_N + m_\Delta = 2.182$  GeV, can be easily simulated and included into our transport model. The only unknown quantity is the cross section of this process. We estimated it by means of the linear

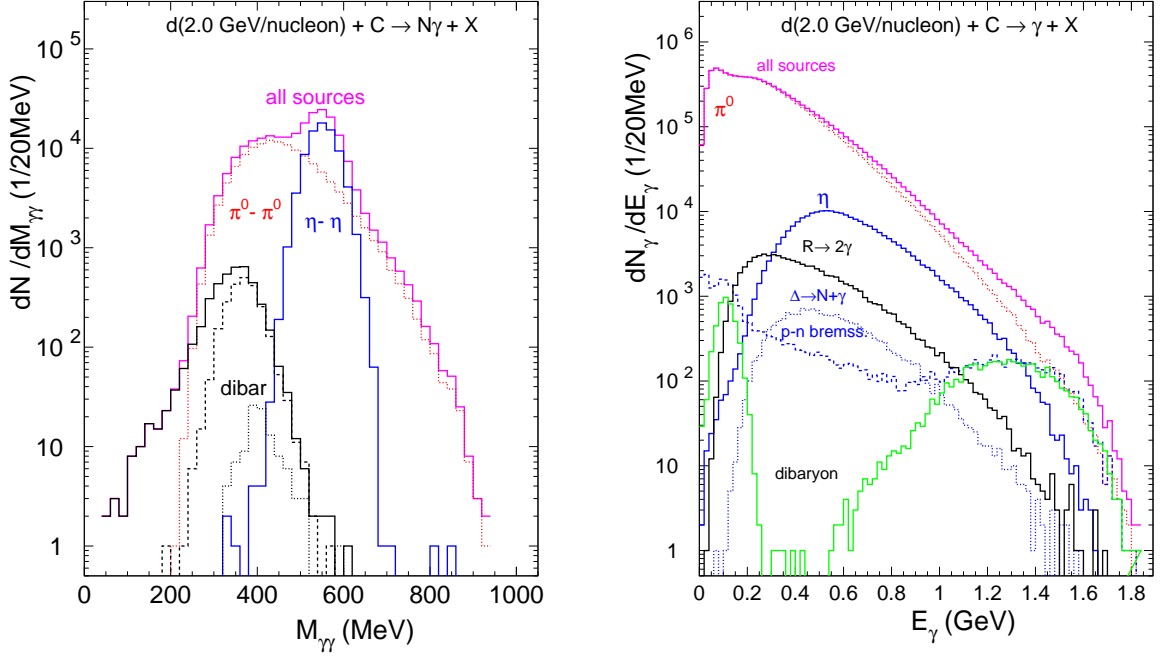


Figure 18: (color online) The  $\gamma\gamma$  invariant mass distribution (left) and energy spectra of photons (right) calculated for  $dC$  collisions with inclusion of the dibaryon mechanism. Contributions of different channels are shown similarly to Fig.16. All curves beside the dibaryon one are given for the PHOTON-2 selected events. For the dibaryon channel (marked as "dibar") the total two photon yield is presented.

extrapolation of the two available points measured at 1.2 and 1.36 GeV [52] till the energy of about 2 GeV.

In Fig.18, such model calculation results with inclusion of the dibaryon channel are presented. If the beam energy of the  $pp$  collision is fixed by 2 GeV, the photon energy at the first step  $pp \rightarrow d_1^* \gamma$  will be a line,  $E_{\gamma 1} = (s - M_d^2)/(2\sqrt{s}) = 640$  MeV in the c.m. system. Here  $s$  is the total  $pp$  colliding energy squared. In the lab. system the maximal photon energy reaches about 1.5 GeV. However, the photon from the second stage will be soft, being defined by the baryon mass. Nevertheless, the maximum position of appropriate two photon distribution moves also with the energy increase. The total photon spectra from dibaryon and other sources from  $dC$  interactions are shown in the right panel of Fig.18 and it has a two-bump structure which mirrors the two-step production mechanism. One should note that in contrast with all other results in this figure the distributions of the dibaryon channel are obtained for the full  $4\pi$  acceptance without any limitation on energy. If the PHOTON-2 selection conditions are implemented to the dibaryon channel, the low energy photons are cut and we get no two-photon pair from the dibaryon among  $10^9$  simulated collisions. Therefore, this dibaryon mechanism cannot explain the observed anomaly.

One should note that in a certain sense the model considered is a conventional dibaryon model where no nonhadronic degrees of freedom are involved. Generally, these results may differ from those obtained within nonconventional dibaryon models like [56].

## 5 Estimate of the $\eta$ and $R$ production cross sections and resonance widths

The summed number of  $pC$ - and  $dC$ -interactions in the experiment amounts to  $\sim 3 \cdot 10^{11}$  and  $\sim 2 \cdot 10^{12}$ , respectively. The inelastic cross sections of the observed  $pC$  and  $dC$  reactions are  $\sigma_{\text{inel}}(pC) = 411$  mb and  $\sigma_{\text{inel}}(dC) = 426$  mb [57], respectively.

The cross section for the  $\eta$  production in  $dC$  collisions (similarly to  $pC$  interactions) is defined as follows:

$$\sigma(dC \rightarrow \eta + X) = \sigma_{\text{inel}}(dC) \cdot \frac{N_{\eta}^{\text{exp}}}{N_{dC\text{-inter}}} \cdot \frac{N_{\text{all } \eta}^{\text{mod}}}{N_{\eta}^{\text{mod}}/K_{\text{opt}}} . \quad (8)$$

Here the first two factors are the reaction cross section and the measured mean multiplicity of  $\eta$  mesons. A number of true  $dC$  interactions resulting in the  $\eta$  production is given as

$$N_{dC\text{-inter}} = K_{\text{empty}} \cdot K_{\text{beam-absorb}} \cdot N_d , \quad (9)$$

where the total number of beam particles passing through the target  $N_d = (1 \div 2.5) \cdot 10^{12}$  is corrected on possible interactions outside the target  $K_{\text{empty}} \sim 0.995$ , to be estimated by a special experiment with an empty target, as discussed in Sect. 2.2, and the beam absorption  $K_{\text{beam-absorb}} = 0.5 \pm 0.2$ . The last factor reflects a particularity of internal beam experiments where the direct monitoring is impossible and part of the initial beam does not interact during the working circle.

The third factor in eq.(8) is the ratio of the total number of simulated  $\eta$  mesons to a number of  $\eta$ 's decaying into two photons under PHOTON-2 experimental conditions. The coefficient  $K_{\text{opt}} = 8.93$  takes into account the rotation of the modelled events in the  $\phi$  plane to find other possible  $\gamma\gamma$  pairs in the given event satisfying the selection conditions. Assuming that photons in the event are distributed homogeneously in  $\phi$ , this trick allows one to increase effectively statistics of the selected events.

So for the  $\eta$  production in  $dC$  collisions we have

$$\sigma(dC \rightarrow \eta + X) = 1.31 \pm 0.11_{-0.89}^{+1.24} \text{ mb} .$$

In the case of  $pC$  collisions we get  $N_p = (1.5 \div 5) \cdot 10^{11}$ ,  $K_{\text{beam-absorb}} = 0.8 \pm 0.2$ , coefficients  $K_{\text{empty}}$  and  $K_{\text{opt}}$  are practically the same as for  $dC$ -collisions, so for the cross section we have

$$\sigma(pC \rightarrow \eta + X) = 3.2 \pm 0.2_{-1.9}^{+4.5} \text{ mb} .$$

Large systematic errors of cross sections are coming mainly from a problem of monitoring the intensity of the internal beam.

The obtained values for cross sections are compared in Fig.19 with calculated excitation functions for the  $\eta$  meson production in the  $pC$  reaction. Note that the DCM model agrees in the absolute scale with the experimental differential cross section for this reaction in the energy range of  $T_p = 0.8 \div 2.0$  GeV (see Fig.11). The measured  $\sigma(pC \rightarrow \eta + X)$  is below theoretical predictions by a factor of about 2. The scaled  $pp$  excitation essentially differs from nuclear one in the near-threshold region due to Fermi motion. The needed scale factor  $A = 12$  is a little bit higher than naively expected  $A^{2/3}$  because these data correspond to the  $pp \rightarrow pp\eta$  channel only while nuclear

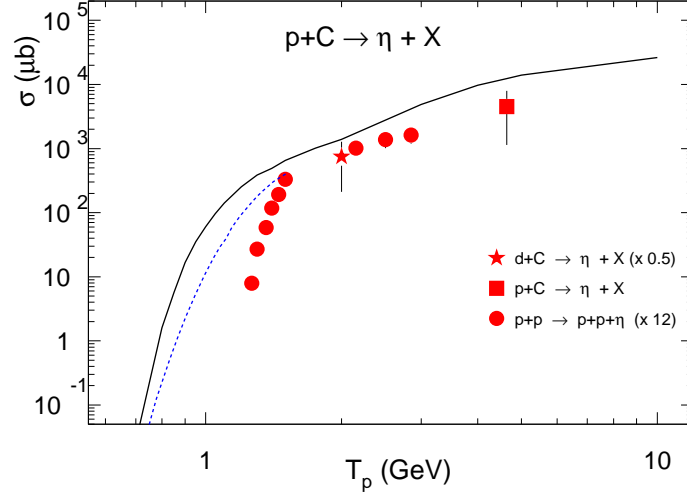


Figure 19: (color online) Excitation function for  $\eta$  production in  $pC$  collisions calculated by Cassing [58] (dotted curve) and within our DCM model (solid line). Our measured points for  $dC$  (with a factor of 0.5) and  $pC$  collisions are plotted by the star and square, respectively. Circles show the cross section for elementary collisions  $pp \rightarrow pp\eta$  multiplied by the factor of 12.

excitation functions include all channels,  $pp \rightarrow \eta + X$ . Unfortunately, there is no other experimental points in this energy range.

If the cross section for the  $\eta$  production is known, the cross section for the  $R$ -resonance may be estimated as follows:

$$\begin{aligned} \sigma(dC \rightarrow R \rightarrow \gamma\gamma) &= \sigma(dC \rightarrow \eta + X) \cdot Br(\eta \rightarrow \gamma\gamma) \cdot \frac{N^{\text{exp}}(R \rightarrow \gamma\gamma)/\epsilon_R}{N^{\text{exp}}(\eta \rightarrow \gamma\gamma)/\epsilon_\eta} = \\ &= (0.075 \pm 0.018) \cdot \sigma(dC \rightarrow \eta + X) = 98 \pm 24_{-67}^{+93} \mu\text{b} , \end{aligned} \quad (10)$$

where the branching ratio is  $Br(\eta \rightarrow \gamma\gamma) = 0.38$ ,  $\epsilon_R = N^{\text{mod}}(R \rightarrow \gamma\gamma)/N_{\text{tot}}^{\text{mod}}(R)$  and  $\epsilon_\eta = N^{\text{mod}}(\eta \rightarrow \gamma\gamma)/N_{\text{tot}}^{\text{mod}}(\eta)$  are the detection and selection efficiency. The measured average reduced multiplicities are compared in Fig.20 with available systematics for meson production near the threshold energies. This simple energy scaling systematics for the subthreshold and near threshold particle production was proposed in [60]. A number of participant nucleons is estimated from the geometrical consideration as

$$\langle A_{\text{part}} \rangle = \frac{A_p A_T^{2/3} + A_T A_p^{2/3}}{(A_p^{1/3} + A_T^{1/3})^2} . \quad (11)$$

The bombarding kinetic energy is corrected for the Coulomb barrier  $V_c$ . This systematics is valid also for  $K$  and  $\rho$  mesons [59, 60]. As is seen, the measured  $\eta$  production points are somewhat below the general trend. Partially, it may be caused also by that all other experimental points correspond to heavier nuclear systems and eq.(11) is not very justified for our reactions.

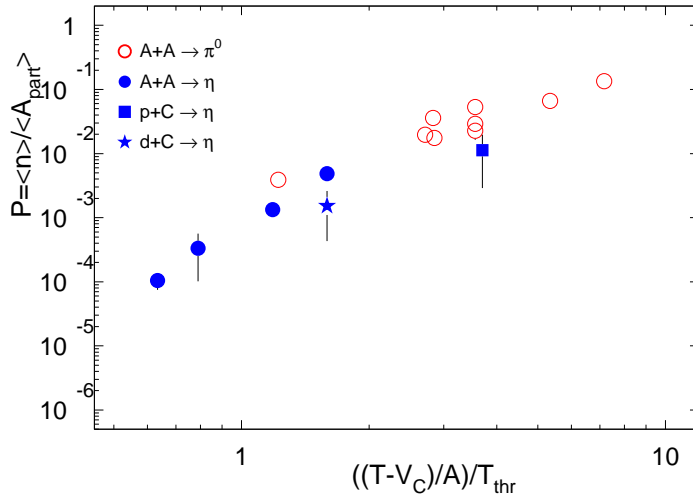


Figure 20: (color online) Meson production probability per participant nucleon as a function of the bombarding energy per nucleon normalized to the respective meson production threshold  $T_{thr}$  in free nucleon-nucleon collisions. Experimental points of the TAPS collaboration are taken from the review [59]. Our points for  $dC$  and  $pC$  collisions are plotted by the star and filled square.

As to the true internal width  $w$  of the observed resonances, they are defined by the measured width  $w_{measur}$  and also specified by the spectrometer resolution  $w_{sp}$  :

$$w = (w_{measur}^2 - w_{sp}^2)^{1/2} . \quad (12)$$

The spectrometer resolution depends on the  $M_{\gamma\gamma}$  range. For the  $R$  and  $\eta$  invariant mass range we have, respectively,

$$\begin{aligned} 2w_{sp}(340 < M_{\gamma\gamma} < 360\text{MeV}) &= 52.6 \text{ MeV}, \\ 2w_{sp}(540 < M_{\gamma\gamma} < 560\text{MeV}) &= 68.6 \text{ MeV}. \end{aligned} \quad (13)$$

So, according to eq.(12), the intrinsic widths of detected resonances are

$$\begin{aligned} 2w(\eta \rightarrow \gamma\gamma) &\approx 0. \\ 2w(R \rightarrow \gamma\gamma) &\simeq 63.7 \pm 17.8 . \end{aligned} \quad (14)$$

As is expected, the width of the  $\eta$ -meson practically equals 0, whereas it essentially differs from zero for the observed resonance. The value of  $2w$  in the Gaussian distribution (3) practically coincides with the width  $\Gamma$  in the Breit-Wigner function; thus, the intrinsic width of the observed resonance structure is about  $64 \pm 18$  MeV.

## 6 Concluding remarks

Thus, based on a thorough analysis of experimental data measured at the JINR Nuclotron and statistics of  $2339 \pm 340$  events of  $1.5 \cdot 10^6$  triggered interactions of a record total number  $2 \cdot 10^{12}$  of  $dC$ -interactions there was observed a resonance-like enhancement

at the mass  $M_{\gamma\gamma} = 360 \pm 7 \pm 9$  MeV, with the width  $\Gamma = 64 \pm 18$  MeV. The production cross section  $\sigma_{\gamma\gamma} \sim 98 \mu b$  is estimated preliminary in the invariant mass spectrum of two photons produced in  $dC$ -interactions at momentum of incident deuterons 2.75 GeV/c per nucleon. A structure like this is not observed in the  $M_{\gamma\gamma}$  spectrum from  $pC$  (5.5 GeV/c) interactions while the  $\eta$  meson is clearly seen in both the cases. These results, obtained by means of the mixing event background, are confirmed by the wavelet analysis.

Due to the use of internal beams of the JINR Nuclotron, totally more than  $10^6$  triggered events at high discriminator thresholds were recorded for every reaction during these experiments. Smallness of the signal-to-background ratio in the  $R$ -resonance mass range needs very high statistics for observation. This demand was not satisfied in previous experiments and therefore no structure has been observed in this invariant mass range. As was noted above, the only most statistically meaningful measurement of the invariant mass spectra was made by the TAPS-collaboration but to resolve the resonance structure discussed, a number of registered events in the TAPS experiment should be increased by an order of magnitude.

To certain extent this enhancement at  $M_{\gamma\gamma} \sim (2 - 3)m_\pi$  is similar to the puzzling ABC effect observed for two-pion pairs from nucleon-nucleon and lightest nuclei collisions at the near threshold energy. In the given work we see that it exists in the  $\gamma\gamma$  channel and measurements are extended to a heavier system. It means that this resonance-like structure is a quite stable object which even survives in the nuclear surrounding.

To understand the origin of the observed structure, several dynamic mechanisms were attempted: production of the hypothetic  $R$  resonance in  $\pi\pi$  interactions during the evolution of the nuclear collision, formation of the  $R$  resonance with participation of photons from the  $\Delta$  decay, the  $\pi^0\pi^0$  interaction effect in the  $3\pi^0$  channel of the  $\eta$  decay, and a particular decoupled dibaryon mechanism. Unfortunately, none of these mechanisms is able to explain the measured value of the resonance-like enhancement, though they contribute to the invariant mass in the region of interest.

The carbon target is really the heaviest one used in experiments where ABC-like structure has been observed. In contrast with all other experiments considered here, one may expect some manifestation of in-medium effects. The prominent feature of the  $\eta$  meson is that the  $\eta$ -nucleon system couples dominantly to the  $N^*(1535)(S^{11})$  resonance at the threshold energies. Hence, due to the  $\eta$  coupling to  $N^*(1535)$ -nucleon-hole modes, one could expect the eta meson nuclear dynamics to be sensitive to modification of nucleon and  $N^*$  properties in medium. As was shown in [61], the  $\eta$  spectral function at normal nuclear density has a second maximum near  $m_\eta \sim 400$  MeV which may be associated to a partial chiral symmetry restoration. Its two-photon decay inside a nucleus might give a rise to a maximum close to the measured value of  $R$ . Unfortunately, we cannot perform transport calculations with taking into account the in-medium modification of hadron properties.

As was noted in Introduction, the recent data of the WASA-CELSIUS Collaboration provide a strong support to the idea of a nontrivial dibaryon state [17, 18]. An attractive candidate for its realization may be a model of the intermediate  $\sigma$ -dressed dibaryon [56]. In this model the short-range  $NN$  interaction, described by the standard  $t$ -channel  $\sigma$  exchange between two nucleons, is replaced with the respective  $s$ -channel  $\sigma$  exchange associated with the intermediate dibaryon production treated as a  $\sigma$ -dressed six-quark bag. The strong scalar  $\sigma$ -field arises around the symmetric  $6q$  bag, because the change



in the symmetry of six-quark state in the transition from the  $NN$  channel to the intermediate dressed-bag state. Due to a strong attraction of the  $\sigma$  meson to quarks, this intensive  $\sigma$  field squeezes the bag and increases its density. The contribution of the  $s$  channel mechanism would be generally much larger than the conventional  $t$ -channel one due to a resonance-like enhancement. The high quark density in the symmetric  $6q$  state enhances meson field fluctuations around the multiquark bag and thereby partially restores the chiral symmetry. Therefore, the mass of  $\sigma$  meson gets much lower and has been estimated to be the value  $m_\sigma \sim 350 \div 380$  MeV. In its turn, it should enhance the near-threshold pion and double-pion production [56, 62]. In addition, a large variety of nuclear data, in particular properties of short- and intermediate-range of  $NN$  and  $3N$  potentials, has been explained within this model; however, still there is no direct quantitative calculations of the ABC-like effects.

From the experimental side it is highly desirable to determine more accurately the mass, width, and cross section of the observed resonance structure by enlarging the acceptance. To verify the above conclusions new experiments are required to be carried out under conditions appropriate for detection of pairs of two photons within the invariant mass interval of 300-400 MeV. In this respect experiments on proton and carbon targets with proton and deuteron beams at the same energy per nucleon would be very useful. Some scanning in the beam energy will clarify the possible resonance structure of this effect. By varying the opening angle of the PHOTON-2 spectrometer it is possible to get information about momentum spectra of the produced resonance-like structure which could be a delicate test of the  $R$  production mechanism.

### Acknowledgements

We thank S.B. Gerasimov, E.E. Kolomeitsev and E.A. Stokovsky for fruitful discussions and reading the manuscript. We are grateful to A.S. Danagulyan, V.D. Kekelidze, A.S. Khrykin, V.I. Kukulkin, V.A. Nikitin, A.M. Sirunyan, O.V. Teryaev, G.A. Vartapetyan for discussions and valuable remarks. Furthermore, we would like to thank S.V. Afanasev, V.V. Arkhipov, A.S. Artemov, A.F. Elishev, A.D. Kovalenko, V.A. Krasnov, A.G. Litvinenko, A.I. Malakhov, S.N. Plyashkevich and the staff of the Nuclotron for their help in conducting the experiment, as well as B.V. Batyunya, A.V. Belozerov and A.G. Fedunov for their help in analyzing data.

The work was supported in part by the Russian Foundation for Basic Research, grant 08-02-01003-a and a special program of the Ministry of Education and Science of the Russian Federation, grant RNP.2.1.1.5409.

**Appendix A. Continuous wavelets with vanishing moments** Here we would like to elucidate some details of the wavelet analysis.

The family of continuous wavelets with *vanishing moments* (VMW) is presented here by Gaussian wavelets (GW) which are generated by derivatives of the Gaussian function (7). For canonical Gaussian with  $x_0 = 0$ ;  $\sigma = 1$  and  $A = 1$  one obtains

$$G_n(a, b) \equiv G_n(x) = (-1)^{n+1} \frac{d^n}{dx^n} e^{-x^2/2}, \quad (15)$$

where  $n > 0$  is the order of the  $g_n(x)$  wavelet. The normalizing coefficients of these wavelets  $C_{g_n}$  are  $2\pi(n-1)!$ .

The most known in the GW family is the second order GW

$$G_2(x) = (1 - x^2)e^{-\frac{x^2}{2}},$$

which is also known as "the Mexican hat" [31].

We use here also GW of higher orders, in particular,

$$G_4(x) = (6x^2 - x^4 - 3)e^{-\frac{x^2}{2}} \quad (16)$$

$$G_6(x) = -(x^6 - 15x^4 + 45x^2 - 15)e^{-\frac{x^2}{2}} \quad (17)$$

$$G_8(x) = -(x^8 - 28x^6 + 210x^4 - 420x^2 + 105)e^{-\frac{x^2}{2}} \quad (18)$$

It is a remarkable fact that the wavelet transformation of Gaussian (7) looks like the corresponding wavelet. Therefore, the general expression for the n-th wavelet coefficient has the following form (see derivations in [30]):

$$W_{g_n}(a, b)g = \frac{A\sigma a^{n+1/2}}{\sqrt{(n-1)!} s^{n+1}} g_n\left(\frac{b-x_0}{s}\right), \quad (19)$$

where we denote  $s = \sqrt{a^2 + \sigma^2}$ .

The parameters  $a$  and  $b$  of continuous wavelets in eq.(4) are changing continuously, which leads to the redundant representation of the data. In some cases, the above mentioned GW properties are quite useful, in particular, this redundant representation facilitates careful spectrum manipulations. The price of this redundancy consists in slow speed of calculations. Besides, all signals to be analyzed have in practice a discrete structure.

It is noteworthy that GW should be used with some care since they are nonorthogonal, which may disturb amplitudes of the filtered signal after their inverse transform. In this respect the discrete wavelet transform looks more preferable for many applications of computing calculations with real data [32] and deserves special consideration. As was noted above, in our particular case of the continuous WVM one can identify resonances without the inverse transformation.

Let us demonstrate this scheme by the  $G_2(a, b)$  wavelet example.

According to eq.(19), one can obtain the maximum (absolute) value of  $G_2$  for a Gaussian (7) at the shift point  $b = x_0$  as

$$\max_b W_{G_2}(a, x_0)g = \frac{A\sigma a^{5/2}}{(a^2 + \sigma^2)^{3/2}}. \quad (20)$$

In the wavelet domain of  $G_2(a, x_0)$  this dependence looks like a simple curve with one maximum. To find it, one has to solve the equation

$$\frac{d}{da} \max_b W_{G_2}(a, x_0)g = 0$$

The corresponding calculations give the position of maximum at the scale axis as  $a_{max} = \sqrt{5}\sigma$ . Since the maximum location in the  $G_2$  domain is stable when the signal is contaminated by some noise (see [30]), one can use the obtained point  $x_0, a_{max}$  to start the fit. Although the maximum of a real contaminated signal is inevitably blurred over some area in the wavelet space due to various distortions, it can nevertheless be used as a good starting point for iterations minimizing a fitting functional.

## References

- [1] A. Abashian, N.E. Booth, and K.M. Crowe, Phys. Rev. Lett.**5**, 3258 (1960); N.E. Booth, A. Abashian, and K.M. Crowe, Phys. Rev. Lett.**7**, 35 (1961); Phys. Rev. **132**, 2309 (1963).
- [2] J. J.Banaigs, J. Berger, L. Goldzahl, T. Risser, L. Vu-Hai, M. Cottureau and, C. Le Brun, Nucl. Phys. **B67**, 1 (1973).
- [3] R.J. R. J. Homer, Q. H. Khan, W. K. McFarlane, J. S. C. McKee, A. W. O'Dell, L. Riddiford, P. G. Williams, D. Griffiths, Phys. Lett. **9**, 72 (1964).
- [4] J.J. H. Hall, T. A. Murray, L. Riddiford, Nucl. Phys. **B12**, 573 (1969).
- [5] I. Bar-Nir et al., Nucl. Phys. **B54**, 17 (1973).
- [6] J. Banaigs, J. Berger, L. Goldzahl, L. Vu Hai, M. Cottureau and, C. Le Brun, F. L. Fabbri and, P. Picozza, Nucl. Phys. **B105**, 52( 1976).
- [7] R. Wurzinger et al., Phys. Lett. **B445**, 423 (1999).
- [8] F. Plouin et al., Nucl. Phys. **B302**, 413 (1978).
- [9] A. Abdivaliev, C. Besliu, F. Cotorobai, A.P. Gasparian, S. Gruia, A.P. Ierusalimov, D.K. Kopylova, V.I. Moroz, A.V. Nikitin, Yu.A. Troyan, Sov. J. Nucl. Phys. **29**, 796 (1979); Nucl. Phys. **B168**, 385 (1980).
- [10] F. Plouin, P. Fleury, and C. Wilkin, Phys. Rev. Lett. **65**, 690 (1990).
- [11] B. Richter, Phys. Rev. Lett. **9**, 217 (1962).
- [12] R. Del Fabbro, M. De Pretis, R. Jones , G. Marini , A. Odian, G. Stoppini , and L. Tau , Phys. Rev. Lett. **12**, 674 (1964).
- [13] M.H. Johnson and E. Teller, Phys. Rev. **98**, 783 (1955).
- [14] A. Codino and F. Plouin, *Production of light mesons and multipion systems in light nuclei interactions*, LNS/Ph/94-06.
- [15] W.-M. Yao et al., J. Phys. **G33**, 1 (2006).
- [16] I. Caprini, G. Colangelo, and H. Leutwyler, Phys. Rev. Lett. **96**, 132001 (2006).
- [17] T. Skorodko et al., CELSIUS-WASA Collaboration, arXiv:nucl-ex/0612016.
- [18] H. Clement, M. Bashkanov, E. Doroshkevich, O. Khakimova, F. Kren, A. Pricking, T. Skorodko, G. J. Wagner, CELSIUS-WASA Collaboration, arXiv:0712.4125., Prog.Part.Nucl.Phys **61**, 276 (2008)
- [19] J. Yonnet et al., Phys. Rev. **C63**,014001 (2001).

- [20] Kh.U. Abraamyan et al., In Proc. of the Int. Workshop "Relativistic Nuclear Physics: from Hundreds MeV to TeV", Dubna, 2005, p.228; Workshop Round Table Discussion: "Searching for the mixed phase of strongly interacting matter at the JINR Nuclotron", JINR, Dubna, 7 - 9 July 2005, <http://theor.jinr.ru/meetings/2005/roundtable/>.
- [21] Kh.U. Abraamyan, A.N. Sissakian, and A.S. Sorin, Observation of new resonance structure in the invariant mass spectrum of two gamma-quanta in  $dC$ -interactions at momentum 2.75 GeV/c per nucleon, nucl-ex/0607027.
- [22] Kh.U. Abraamyan, V.M. Izyurov, M.N. Khachatourian, M.A. Kozhin, G. L. Melkumov, A. H. Khudaverdyan, Phys. Lett. **B323**, 1 (1994); Yad. Fiz. **59**, 271 (1996)(translated as Phys. Atom. Nucl. **59**, 252 (1996)); **60**, 2014 (1997)(translated as Phys. Atom. Nucl. **60**, 1843 (1997)); **68**, 1020 (2005) (translated as Phys. Atom. Nucl. **68**, 982 (2005)).
- [23] Kh.U. Abraamyan et al., Instruments and Experimental Techniques **32**, 58 (1989); **39**, 775 (1996).
- [24] M.N. Khachatourian, JINR Communication E1-85-55, Dubna, 1985; R.G. Astvatsaurov et. al., Nucl. Instr. Methods, **163**, 343 (1979).
- [25] V.T. Stane and Ch. Vankov Ch. Comput. Phys. Comm. **16**, 363 (1979).
- [26] R. Averbeck et al., TAPS Collaboration, Z. Phys. A **359**, 65 (1997).
- [27] M. Holschneider, *Wavelets: An analysis tool*, Oxford University Press, Oxford, 1995.
- [28] B. Torresani, *Analise continue par ondelettes*, Savoirs actuels, Savoirs Actuels, Paris, 1995.
- [29] I. Daubechies, The wavelet transform, time frequency localization and signal analysis, IEEE Trans. Inform. Theory **36**, 961 (1990).
- [30] G. Ososkov and A. Shitov, Comp. Phys. Comm, **126**, 149 (2000).
- [31] D. Donoho, Amer. Math. Soc., Providence, R.I., **47**, 173 (1993).
- [32] S.A. Mallat, Theory for multi-resolution signal decomposition: the wavelet representation. IEEE Trans. Pattern Analysis and Machine Intelligence, (1989).
- [33] I.M. Dremin, O.V. Ivanov, and V.A. Nechitailo, Uspekhi Fiz. Nauk, **171**, 465 (2001) (in Russian), Phys. Usp. **44**, 447 (2001).
- [34] N.M. Astafieva, Uspekhi Fiz. Nauk, **166**, 1145 (1996) (in Russian), Phys. Usp. **39**, 1085 (1996).
- [35] T.S. Belozerova, P.G. Frick, and V.K. Henner, Yad. Fiz. **66** (2003) (translated as Phys. Atom. Nucl. **66**, 1309 (2003)).

- [36] N.S. Amelin, K.K. Gudima, and V.D. Toneev, Sov. Journ. of Nuclear Phys. **51**, 1730 (1990); N.S. Amelin et al., Sov. Journ. of Nuclear Phys. **52**, 172 (1990); Phys. Rev. **C44**, 1541 (1991); V.D. Toneev et al., Nucl.Phys. **A519**, 463 (1990); N.S. Amelin et al., Phys. Rev. Letters **67**, 1523 (1991); V.D. Toneev et al, Sov. J. of Nucl. Phys. **54**, 1272 (1992); N.S. Amelin et al., Phys. Rev. **C47**, 2299 (1993).
- [37] V.D. Toneev and K.K. Gudima. Nucl. Phys. **A400**, 173 (1983).
- [38] K. K. Gudima, S. G. Mashnik, and A. J. Sierk, LANL Report LA-UR-01-6804, Los Alamos, 2001.
- [39] K.K. Gudima, S.G.Mashnik and V.D.Toneev, Nucl. Phys. **A401**, 329 (1983).
- [40] V.D. Toneev, N.S. Amelin, K.K. Gudima, and S.Y. Sivoklokov, Nucl. Phys. **A519**, 463 (1990).
- [41] N.S. Amelin, K.K. Gudima, and V.D. Toneev, Sov. J. Nucl. Phys. **52**, 172 (1990).
- [42] G. Agakishiev et al., HADES Collaboration, Phys. Rev. Lett. **98**, 052302 (2007); Phys. Lett. **B663**,43 (2008)
- [43] L.P. Kaptari, B. Kämpfer, Nucl. Phys. **A764**, 338 (2006).
- [44] E.L. Bratkovskaya and W. Cassing, Nucl. Phys. **A807**, 214 (2008)
- [45] E. Chiavassa, G. Dellacasa, N. De Marco, F. Ferrero, M. Gallio, P. Guaita, A. Musso, A. Piccotti, E. Scomparin, E. Vercellin, Z. Phys. A **342**, 107 (1992); Nucl. Phys. **A538**, 121 (1992).
- [46] T. Risser and M.D. Shuster, Phys. Lett. **B43** (1973) 68; I. Bar-Nir, T. Risser and M.D. Shuster, Nucl. Phys. **B87**, 109 (1975); J.C Anjos, D. Levy and A. Santoro, **B67**, 37 (1973).
- [47] A. Gardestig, C. Feld, and C. Wilkin, Phys. Rev. **C59**, 6208 (1999); Phys. Lett. **B421**, 41 (1998).
- [48] L.M. Brown and P. Singer, Phys. Rev. Lett. **8**, 460 (1962).
- [49] F.S. Crawford, Jr., R.A. Grossman, L.J. Lloyd, L.R. Price and E.C. Fowler, Phys. Rev. Lett. **11**, 564 (1963).
- [50] A. Roy for CBELSA TAPS Collaboration, PRAMANA - J. of Phys., **66**, 921 (2006).
- [51] K. Nishijima, Phys. Rev. Lett. **12**, 39 (1964).
- [52] M. Bashkhanov et al., Int. J. of Mod. Phys. **A20** (2005) 554; Observation of a structure in  $pp \rightarrow pp\gamma\gamma$  near the  $\pi\pi$  threshold and its possible interpretation by  $\gamma\gamma$  radiation from chiral loops in the mesonic  $\sigma$  channel, arXiv:hep-exp/0406081.
- [53] A.S. Khrykin and S.B. Gerasimov, On a possible origin of a resonance-like structure in the two-photon invariant mass spectrum of the reaction  $pp \rightarrow pp\gamma\gamma$ , arXiv:0710.3331.

- [54] A.S. Khrykin, V.F. Boreiko, Yu.G. Budyashov, S.B. Gerasimov, N.V. Khomutov, Yu.G. Sobolev, and V.P. Zorin, Phys. Rev. **C64**, 034002 (2001); Nucl. Phys. **A721**, 625 (2003).
- [55] A. Matsuyama, Phys. Lett. **B 408**, 25 (1997).
- [56] V.I. Kukulín and M.A. Shikhalev, Phys. At. Nucl. **67**, 1536 (2004); A. Faessler, V.I. Kukulín and M.A. Shikhalev, Ann. Phys. **320**, 71 (2005); V.I. Kukulín, I.T. Obukhovskiy, V.N. Pomerantsev and A. Faessler, Int. J. Mod. Phys. **E11**, 1 (2002).
- [57] V.S. Barashenkov, Cross-sections of interactions of particles and nuclei with nuclei. Dubna, 1993; V.S.Barashenkov and V.D.Toneev, *High Energy Interaction of Particles and Atomic Nuclei with Nuclei*, Atomizdat, Moscow, 1972 (in Russian).
- [58] W.Cassing, G. Batko, T. Vetter, and G. Wolf, Z. Phys. **A340**, 51 (1991).
- [59] W. Kuhn, Czech. J. Phys. **45**, 537 (1995).
- [60] V. Metag, Prog. Part. Nucl. Phys. **30**, 75 (1993).
- [61] D. Jido, E.E. Kolomeitsev, H. Nagahiro, and S. Hirenzaki, Nucl. Phys. **A811**, 158 (2008); arXiv:0801.4834.
- [62] V.I. Kukulín, V.N. Pomerantsev, M. Kaskulov and A. Faessler, J. Phys. **G30**, 287 (2004); J. Phys. **G30**, 309 (2004).